2023

Subsurface Structure And Impacts Of Marine Heatwaves In The Chesapeake Bay

Nathan P. Shunk
William & Mary - Virginia Institute of Marine Science, nathan.shunk42@gmail.com

Subsurface Structure and Impacts of Marine Heatwaves in the Chesapeake Bay

A Thesis

Presented to

The Faculty of the School of Marine Science

The College of William & Mary in Virginia

In Partial Fulfillment

of the Requirements for the Degree of

Master of Science

by

Nathan Paul Shunk

August 2023

APPROVAL PAGE

This thesis is submitted in partial fulfillment of

the requirements for the degree of

Master of Science

Nathan Paul Shunk

Approved by the Committee, August 2023

Piero L. F. Mazzini, Ph.D.
Committee Chair / Advisor

Carl T. Friedrichs, Ph.D.

Marjorie A. M. Friedrichs, Ph.D.

Mark J. Brush, Ph.D.

TABLE OF CONTENTS

ACKNOWLEDGEMENTS

Firstly, I want to express my gratitude towards my advisor, Dr. Piero Mazzini, who has been an excellent mentor and steadfast proponent of my personal and professional growth. Piero has been my guide as I built up my confidence in my work and showed me how to broaden my focus from the immediate data analysis to the larger story and how that analysis fits in (though I do still love troubleshooting code). He has pushed, challenged, and supported me by facilitating and encouraging the various supplemental experiences (e.g., field work, teaching, outreach, etc.) I participated in alongside my education and research and I am eternally grateful.

Secondly, I wish to thank my committee and other collaborators for their help in shaping and guiding my work. My committee members, Drs. Carl Friedrichs, Marjy Friedrichs, and Mark Brush, were invaluable in shaping and refining my research in the second year of my program. Carl, thank you for your insights on statistical and climatological analysis, which shaped my final subsurface analyses. Marjy, thank you for your guidance through the degree milestones, which was extremely helpful with navigating the VIMS degree process, and your insights on dissolved oxygen. Mark, thank you for sharing your expertise in chlorophyll dynamics in the Bay and helping me interpret my chlorophyll results. Additionally, I want to thank Drs. Cassia Pianca, Julie Reichert-Nguyen, Ryan Walter, and Qubin Qin for their various roles in supporting and shaping the framework, analysis, and writing of this work.

I also want to thank the researchers and staff, both past and present, of the Chesapeake Bay Program, National Data Buoy Center, Center for Operational Oceanographic Products and Services, Chesapeake Bay National Estuarine Research Reserve, US Geologic Survey, VIMS, and their funding sources for collecting and maintaining the vast amount of publicly available monitoring data on which this project relied. If it were not for the tireless efforts of these dedicated researchers and staff members, I would be unable to attempt the type of analysis conducted in this work.

Additionally, I wish to thank the VIMS community, the Office of Academic Studies, and the VIMS Foundation for their support. Thank you to all of the administrative staff that have assisted me with travel, funding and academic logistics—Cynthia Harris, Maxine Butler, Cathy Cake, Jen Hay—and a special thank you to Linda Schaffner who, with the VIMS Foundation, helped secure funding for my time at VIMS. The VIMS community was and still is exceedingly welcoming and I have enjoyed my time here during my master's degree.

Finally, I wish to thank my family and friends who have encouraged and supported me all the way to the finish line. Thank you, Mom and Dad, for encouraging and pushing me to excel even when I was uncertain if I could. Thank you, Zach, Stephen, and Emma, for rooting for me. To my friends, thank you for your support, and for getting me out of the office and home. Finally, Georgia, I want to thank you for your constant support and proofreading, I would not have been able to write this without your help.

LIST OF TABLES

LIST OF FIGURES

ABSTRACT

Extreme temperature events known as Marine Heatwaves (MHW), akin to atmospheric heatwaves, have only recently received attention by the estuarine scientific community. Thus far, studies have focused solely on surface events due to scarcity of long-term subsurface data. This study investigates, for the first time, the subsurface temperature and dissolved oxygen (DO) anomalies associated with surface MHW events in a large, temperate, partially mixed estuary: the Chesapeake Bay (CB). Using over three decades (1986-2021) of in-situ data from several long-term monitoring programs in the CB (including sub daily moored measurements and monthly/bimonthly cruises along the main stem) and a global atmospheric reanalysis product (ERA5), I were able to 1) characterize the spatiotemporal structure of subsurface temperature and DO anomalies during surface MHW events on seasonal time scales, 2) identify the vertical extent of warming before and after events, and 3) examine the relative role of atmospheric heat flux in driving temperature changes during the onset and decline of events. I found that subsurface temperature anomalies associated with surface MHWs had two distinct regimes: a thermally stratified spring-summer regime, when positive temperature anomalies were only present in the upper water column capped by the surface mixed layer; and a thermally homogenous fall-winter regime, when temperature anomalies extended throughout the water column. This seasonal variability in temperature anomalies was largely consistent with a simple 1-D response to heat, sourced primarily through the air-estuary interface, and with downward heat transport and diffusion controlled by seasonally variable stratification and mixing. Moreover, DO anomalies during MHW events presented a more complex spatiotemporal structure, with notable DO decreases (1-4 mg L^{-1}) primarily occurring in the winter and spring. While negative DO anomalies were present across the main stem of the CB, the greatest DO decreases (~5 mg L^{-1}) were observed in the upper region of CB below the mixed layer depth. During the hypoxic season (May to September), and in April and October, negative DO anomalies were often associated with an expansion of the hypoxic zone. Additionally, I observed that subsurface temperature anomalies were elevated 5-10 days before and up to 20 days after MHW events, while surface temperature anomalies were elevated for up to 2 months before and after events. This indicates that the timescales of elevated temperatures are typically much longer than the duration of individual MHW events, and therefore should be carefully taken into consideration when assessing the impact of these extreme events in the estuarine ecosystem. Using a simple 1D surface mixed layer heat budget, I identified air-estuary heat flux as the largest driver of the onset and decline of MHW events, with latent heat flux being the dominant constituent. In the CB, concurrent low DO during MHW events and persistent high temperatures before, during, and after events can compound the impacts of MHWs on habitat, which will be further exacerbated by climate change, severely impacting this valuable estuarine ecosystem.

Subsurface Structure and Impacts of Marine Heatwaves in the Chesapeake Bay

1. Introduction

Long-term temperature trends, and their impacts on ecosystems, have been a subject of extensive research in estuarine systems worldwide (Ashizawa and Cole 1994; Cronin et al. 2003; Preston 2004; Najjar et al. 2010; Seekell and Pace 2011; Oczkowski et al. 2015; Snyder et al. 2019; Hinson et al. 2021; St.Laurent et al. 2021). However, short-lived, extreme temperature events called Marine Heatwaves (MHWs), akin to atmospheric heatwaves, have received significantly less attention in estuarine scientific literature (Shields et al. 2018; Alosairi et al. 2020; Brauko et al. 2020; Mazzini and Pianca 2022; Magel et al. 2022; Tassone et al. 2022; Marin Jarrin et al. 2022; Cook et al. 2022), despite their known impacts in these productive and valuable ecosystems. Mazzini and Pianca (2022) analyzed over three decades of continuous *in-situ* surface temperature data to investigate MHWs in the largest estuary in the continental US, the Chesapeake Bay (CB), resulting in novel insights into the physical characteristics of MHWs and their time variability in this system. They found that the frequency of MHW events is rapidly increasing, following a similar trend observed in the global oceans (Frölicher et al. 2018; Oliver et al. 2019). Moreover, Mazzini and Pianca (2022) showed that the detected trends in the CB can be attributed to long-term global warming, which increases the likelihood of temperatures surpassing the MHW threshold, and if these trends persist, CB will reach a semi-permanent MHW state by the end of the century, whereby presently extreme temperatures would be present for over half of the year.

Overwhelming evidence has demonstrated that extreme temperatures during MHWs can have dire consequences on a wide range of pelagic and benthic ecosystems with lasting ramifications (Oliver et al. 2019; Suryan et al. 2021). Sessile benthic species have been devastated by MHWs with mass die offs of species including: submerged aquatic vegetation (Ehlers et al. 2008; Shields et al. 2018; Strydom et al. 2020; Filbee-Dexter et al. 2020; Aoki et al. 2021; Bass et

al. 2023), mussels (Seuront et al. 2019), scallops, crabs and other benthic invertebrates (Caputi et al. 2016; Pansch et al. 2018; Tomasetti et al. 2023) in addition to global-scale coral bleaching events (Hughes et al. 2017; Eakin et al. 2019). Fin fishes and other pelagic organisms have also faced population declines and large biogeographic shifts due to MHWs (Lonhart et al. 2019; Sanford et al. 2019; Cheung and Frölicher 2020; Colombano et al. 2022). Additionally, MHWs have been associated with large coastal harmful algal blooms, inducing the deaths of higher trophic organisms (McCabe et al. 2016; Trainer et al. 2020). Through these various effects, both fisheries and aquaculture have been impacted by MHWs (Caputi et al. 2016; McCabe et al. 2016; Cheung and Frölicher 2020) with ecosystems only recovering slowly after events (Suryan et al. 2021). Furthermore, impacts from MHW events can compound and exacerbate underlying issues within ecosystems (Brauko et al. 2020; Tassone et al. 2022; Lucey et al. 2022; Tomasetti et al. 2023; Bass et al. 2023). For instance, in Santa Catarina Island, Brazil, Brauko et al. (2020) showed that MHWs induced the first recorded anoxic event in an embayment with preexisting water quality issues due to excessive nitrogen loading and eutrophication.

In the CB, in addition to increasing temperatures, there are higher chlorophyll-a levels due to eutrophication and long-term decreases in dissolved oxygen (DO; which have started to show successful mitigation in recent years), which have led to prolonged periods of summertime hypoxia and anoxia (Kemp et al. 2005; Murphy et al. 2011; Cloern et al. 2014; Ni et al. 2019; Malone and Newton 2020; Frankel et al. 2022). Eutrophication, and subsequently hypoxia, in the CB, are primarily driven by the Susquehanna River nutrient load during the peak spring discharge (Kemp et al. 2005; Li et al. 2016; Malone and Newton 2020). Climate change could exacerbate hypoxic conditions in the CB by a combination of (a) increasing early summer stratification due to sea level rise and increased river flow (though sea level rise could also oxygenate the Bay by increasing

exchange flow, and a consensus on river discharge trends has not been reached); (b) reducing the solubility of DO due to warming waters (e.g., deoxygenation); and (c) increasing oxygen demand due to the combined effects of rising temperatures and higher nutrient loads from increased river flow (Murphy et al. 2011; Irby et al. 2018; Ni et al. 2019; Cai et al. 2021; Hinson et al. 2023). These long-term changes in CB water quality are well documented, but little is known about the impact of MHWs on estuarine water quality, particularly DO, and how these extreme events may compound underlying water quality issues.

While Mazzini and Pianca (2022) investigated MHWs in the surface waters of the CB, their research did not address the impact of MHWs on subsurface waters. In fact, little is known about subsurface MHWs globally due to the overall scarcity of subsurface data with appropriate sampling frequency (daily or higher) and record length (multidecadal); the majority of MHW studies have been limited to the surface of global oceans due to the availability of long sea surface temperature (SST) satellite records (Holbrook et al. 2019; Marin et al. 2021). These records, however, are unable to capture the subsurface structure and dynamics of MHW events because they only represent the SST values (Lee et al. 2010). Nevertheless, a few noteworthy studies (e.g., Schaeffer and Roughan 2017; Hu et al. 2021) have been able to identify MHWs in the subsurface using observations from buoys with daily temperature data (though such records are rare) and with hindcast models (Chen et al. 2015; Oliver et al. 2018; Ryan et al. 2021; Großelindemann et al. 2022; Amaya et al. 2023a). Additionally, less frequently sampled datasets, (i.e., Argo floats, animal mounted sensors, and CTD casts) have been used to examine the subsurface temperature anomalies during identified surface events, allowing for an initial look at the subsurface temperature structure associated with MHWs (Jackson et al. 2018; Freeland and Ross 2019; Elzahaby and Schaeffer 2019; Scannell et al. 2020; Holser et al. 2022). These studies have shown

that MHWs in the global oceans have the potential to last longer and at a greater intensity (e.g., positive temperature anomalies) than what is indicated by their surface signature, thereby increasing the potential impact on marine ecosystems. Yet, the studies discussed above focused on the oceanic environment, with none taking place in estuarine systems, even though estuarine systems could amplify the impacts of MHWs (Oczkowski et al. 2015) on benthic ecosystems given the influence of variable buoyancy influxes via freshwater discharge and strong biogeochemical cycling.

Due to the prolific amount of historical data available, the CB offers an excellent natural laboratory to investigate the subsurface impacts of MHWs in an estuarine system. Combining over three decades of continuous surface temperature measurements from fixed stations with monthly/bimonthly shipboard hydrographic profiles, the present study seeks to investigate the vertical and along-channel structure of temperature anomalies in the CB main stem during MHW events detected at the surface, their seasonal variability, and their impacts on DO. Moreover, understanding the spatial distribution of temperature anomalies associated with MHW events allows for the application of a simple 1-D surface mixed-layer (SML) heat budget model to further investigate the potential role of air-sea heat fluxes in driving the onset and decline of these events. To our knowledge, this is the first study to consider subsurface temperature and dissolved oxygen anomalies during MHW events in an estuarine environment.

2. Methods

2.1 Study Site

The CB is an extremely productive partially mixed estuary (Cloern et al. 2014) and is the largest estuary in the continental United States with a watershed size of 166,319 km^2, an estuary

surface area of 11,655 km^2 (Rice and Jastram 2015), a mean depth of 7 m, and a maximum depth reaching approximately 53 m (Xiong and Berger 2010). Eighty percent of the total freshwater input of the Bay comes from the Susquehanna, Potomac, and James Rivers, and nearly half of the total freshwater input comes from the Susquehanna alone (Schubel and Pritchard 1986; Xiong and Berger 2010). River discharge (Schubel and Pritchard 1986), tides (Zhong and Li 2006; Guo and Valle-Levinson 2007; Xiong and Berger 2010), and winds (Wang 1979; Garvine 1985; Valle-Levinson et al. 2001; Scully 2010a; Li and Li 2011) collectively drive circulation in the CB, with large scale climate forcing — Bermuda High Index and North Atlantic Oscillation — influencing decadal variability (Scully 2010b; Du and Shen 2015). However, seasonal and interannual variation in river discharge is the dominant driver of circulation variability (Schubel and Pritchard 1986). Additionally, the CB has a long residence time — ~180 days — that varies seasonally, and is up to 280 days at depth (Du and Shen 2016). The CB experiences eutrophication and subsequently seasonal hypoxia and anoxia, which are primarily driven by the Susquehanna nutrient load during the peak spring discharge (Kemp et al. 2005; Malone and Newton 2020). Additionally, hypoxia and anoxia in the Bay are modified by the winds and other physical processes (Scully 2010b; Lee et al. 2013; Li et al. 2016; Scully 2016a). Over the last five decades the CB estuary and watershed have seen significant warming, due to global climate change. Estuary temperatures have increased approximately 0.22 and 0.19^oC per decade at the surface and bottom respectively, while watershed stream and air temperatures have increased approximately 0.28^oC and 0.23^oC per decade respectively (Rice and Jastram 2015; Hinson et al. 2021). On average, two MHWs occur per year in CB, typically lasting 11 days (range of 5-50 days) with a mean intensity of 3^oC and appear most frequently in the summer, though events do occur in all seasons (Mazzini and Pianca

2022). Additionally, these events have been increasing in frequency, with the maximum frequency seen in the last decade, reaching up to eight events in some years (Mazzini and Pianca 2022).

2.2 Data

Hydrographic and Water Quality

Six *in-situ* surface temperature time series from a collection of buoys and fixed stations, analyzed by Mazzini & Pianca (2022), from three monitoring programs — the National Data Buoy Center (NDBC), the Center for Operational Oceanographic Products and Services (CO-OPS), and the Chesapeake Bay National Estuarine Research Reserve (CBNERR) — were used to construct a spatially-averaged, daily surface temperature time series representative of CB (See section *2.3 Surface Marine Heatwave Identification*). Located at Tolchester Beach, Thomas Point, Solomons Island, Lewisetta, Goodwin Islands, VIMS (Virginia Institute of Marine Science) pier, and Kiptopeke (Figure 1a), these time series have record lengths of 25 to 35 years, starting between 1986-1998 and analyzed here through 2021, with sampling frequencies ranging from every six minutes to hourly (Table 1). Following Mazzini and Pianca (2022), each time series was low-pass filtered with a 33-hour cutoff to remove tidal and diurnal variability, and subsequently binned to daily values. In addition, the Goodwin Island time series was extended from 1998 to 1986 with the VIMS pier data (Anderson 2021); gaps in all the time series were filled using linear interpolation and SST data from the Multiscale Ultra-high Resolution (MUR) SST Analyses (v4.1) (JPL-MUR-MeaSUREs-Project 2015) from the Physical Oceanography Distributed Active Archive Center (PODAAC) using the same methods as in Mazzini and Pianca (2022).

Subsurface temperature, salinity, and DO data from the Chesapeake Bay Program (CBP) cruise *in-situ* profiles were used to calculate subsurface anomaly profiles. These profiles were

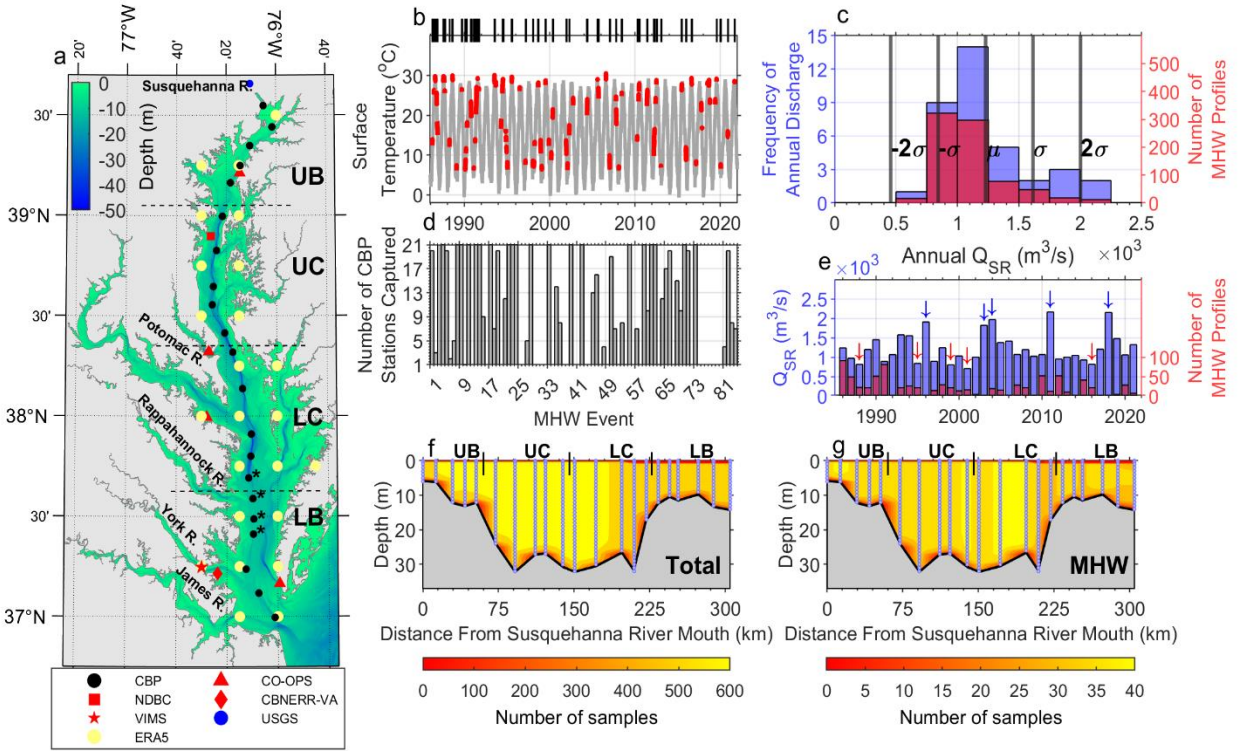

Figure 1. Data Availability and Summary. (a) Bathymetry map of CB including the subsurface monthly profiles sampled by CBP partners (black), surface daily temperature time series (red), daily river discharge (blue), and C3S ERA5 reanalysis heat flux data stations (yellow). CB has been divided into four regions, Upper Bay (UB), Upper Channel (UC), Lower Channel (LC), Lower Bay (LB), based on bathymetry. For reference, the CBP stations with an asterisk on the map (a) indicate the Rappahannock Shoals. (b) Spatially averaged detrended surface temperature time series (grey) and identified MHW days (red) and MHW profiles (bars). (c) The distribution of annual discharge (blue) and MHW profiles (red) sampled in each discharge bin between 1986 to 2021 and the mean annual discharge and two standard deviations (grey line). (d) The number of CBP stations represented during each MHW event identified. (e) Annual discharge (blue) and number of MHW profiles sampled (red) each year from 1986 to 2021 with wet years indicated as a blue arrow and dry years as a red arrow. Total number of CBP samples (f) and number of MHW CBP samples identified (g) at each depth interpolated grid point. Abbreviations: Chesapeake Bay Program (CBP), the Center for Operational Oceanographic Products and Services (CO-OPS), National Data Buoy Center (NDBC), Chesapeake Bay National Estuarine Research Reserve, Virginia (CBNERR-VA), Virginia Institute of Marine Science (VIMS), US Geological Survey (USGS), Copernicus Climate Change Services (C3S).

collected from 21 fixed cruise stations (Figure 1a) sampling monthly/bimonthly by CBP partners — Maryland (MD) Department of Natural Resources (MDDNR) in MD and Old Dominion University (ODU) and VIMS in Virginia (VA) — since 1984 along the CB main stem (Table 1, Figure 1a). These stations were grouped into four regions based on bathymetry: the shallow upper Bay (UB), the deep upper (UC) and lower (LC) channel, and the lower Bay (LB), beginning at the

Rappahannock shoals (see Figure 1a). At each station, temperature, salinity and DO measurements were obtained at fixed depths below the surface of 0.5, 1, 2, 3, and subsequently every 2 m by MDDNR in MD and at 1-2 m intervals from 1 m below the surface to 1 m above the bottom by ODU and VIMS in VA (Table 2). YSI or Hydrolab® Sondes were used by MDDNR, ODU, and VIMS to collect DO profiles, while temperature and salinity were measured by either Applied Microsystems CTD casts (VIMS) or Sonde casts (MDDNR and ODU; Table 2). Transect profiles across the CB typically took around four days to complete and resulted in approximately 500 to 600 *in-situ* profiles per station available to be used in the analysis, with the greatest number of profiles available in the UC and UB (Figure 1f; CBP 2017).

Daily Susquehanna River discharge from the United States Geological Survey (USGS) Conowingo, MD, gauge station was used to account for the potential influence of wet years and dry years on subsurface anomalies (Table 1, Figure 1a). Annual averages of discharge were taken from 1986 to 2021, and a wet or dry year was defined as having annual discharge greater than (wet year) or less than (dry year) one standard deviation from the interannual mean discharge. This resulted in eleven years between 1986 and 2021 being considered anomalously wet or dry (Figure 1c): 5 wet years (1996, 2002, 2003, 2011, and 2018) and 6 dry years (1988, 1995, 1997, 1999, 2001, and 2016) (Figure 1e).

Atmospheric

The air-sea heat flux components—net long-wave radiation (Q_{LR}), net short-wave radiation (Q_{SR}), sensible heat flux (Q_{SH}), and latent heat flux (Q_{LH})—were obtained from the ERA5 reanalysis product from the Copernicus Climate Change Service (C3S) at the European Centre for Medium-Range Weather Forecasts (Hersbach et al. 2018). ERA5 has hourly output and a spatial

Table 1. Data Sources. Summary of the six composite surface time series used in the spatially averaged time series, the subsurface profiles, and atmospheric data used. Daily Susquehanna River discharge is Q_R

Data	Data Type	Availability	Spatial Resolution / Number of Stations	Temporal Resolution	Variables	Source(s)
in-situ Profiles	*in-situ*	1984 - Present	21 Stations	Monthly/ Bimonthly	Temperature, Salinity, DO	CBP
Surface Time Series	*in-situ*/ Satellite	1994/95 - Present	4 Stations	Hourly	Temperature	CO-OS, MUR
Surface Time Series	*in-situ*/ Satellite	1986 - Present	1 Station	Hourly	Temperature	NDBC, MUR
Surface Time Series	*in-situ*/ Satellite	1986 - Present	1 Station	15 Min, 6 Min	Temperature	CBNERR-VA, VIMS, MUR
Susquehanna Discharge	*in-situ*	1967 - Present	1 Station	Daily	Q_R	USGS
ERA5	Reanalysis	1950 - Present	¼° Grid (24 Points used)	Hourly	Q_{SH}, Q_{LH}, Q_{LR}, Q_{SR}	C3S/ECMWF

Table 2. Chesapeake Bay Program (CBP) Profiles Sources. Summary of CBP sources for the subsurface temperature, salinity, and dissolved oxygen (DO) profiles.

	MDDNR	ODU	VIMS
Temperature	YSI Series 6	Hydrolab® Surveyor II (1986-1997) YSI Sonde (1997 - Present)	Applied Microsystems CTD
Salinity	YSI Series 6	Hydrolab® Surveyor II (1986-1997) YSI Sonde (1997 - Present)	Applied Microsystems CTD
DO	YSI Series 6	Hydrolab® Surveyor II (1986-1997) YSI Sonde (1997 - Present)	YSI Sonde
Depth	Levels 0.5, 1, 2, and 3m and every 2m to bottom	Every meter until 15m; every two meters from 15m to bottom	Same as ODU (1986) Ever meter with CTD
Years	1984 – Present	1984 – Present	1984 – 1995
CBP Stations	CB1.1, CB2.1, CB2.2, CB3.1, CB3.2, CB3.3C, CB4.1C, CB4.2C, CB4.3C, CB4.4, CB5.1, CB5.2, CB5.3	CB5.4, CB5.5, CB6.1, CB6.2, CB6.3 (1996 – Present) CB6.4, CB7.3, CB7.4 (1984 – Present)	CB5.4, CB5.5, CB6.1, CB6.2, CB6.3

resolution of 0.25 degree (Table 1); grid points located within the CB main stem were selected and used in the analysis (Figure 1a). The heat flux terms were averaged from noon to noon, centered on midnight, when obtaining daily mean heat flux (Schlegel et al. 2021). This allowed the integral of each heat flux term over a MHW phase to be centered on noon (See Section *2.5 Surface Mixed Layer Heat Budget*).

2.3 Surface Marine Heatwave Identification

I utilized the Hobday et al. (2016) definition of a MHW, where an event is considered a MHW when temperature values from a daily temperature time series are greater than the 90th percentile threshold above the daily climatology for a minimum duration of five days. From the six daily surface temperature time series, a single spatially averaged surface temperature time series was constructed to identify MHWs across the entire CB. The spatially averaged time series is considered representative of the extreme surface temperatures in the main stem of the CB due to the large co-occurrence (50-65%) of MHW events found across the upper, middle and lower Bay (as defined by Mazzini and Pianca (2022)) with respective short time lags (on average ~2 days) across the entire Bay (Mazzini and Pianca 2022), which indicates that the majority of MHWs encompass the entire CB nearly synchronously. Additionally, a spatially averaged time series filters the proportionally smaller, localized effects of the individual temperature time series and instead captures the large-scale forcing driving MHWs across the entire length of the CB main stem.

Before calculating the climatology and 90th percentile threshold, the surface temperature time series was detrended to remove the effect of long-term Bay warming (Hinson et al. 2021; St.Laurent et al. 2021) on MHW identification (Jacox 2019; Amaya et al. 2023b). Trends in the

temperature time series introduce the greatest variability into the results of MHW metric calculations, greater than missing data or time series shorter than 30 years (Schlegel et al. 2019) and are driving MHW metric trends, specifically the increased frequency of events, in the global oceans (Oliver 2019) and in the CB (Mazzini and Pianca 2022). Since MHW profiles were identified as being sampled during a surface MHW event, an increased number of MHW days identified in the last decade of the time series would bias the MHW profiles to the conditions of the last decade. This is important since oxygen levels have generally decreased since the beginning of the time series while temperatures have increased (Murphy et al. 2011). Removing the trend from the data reduces the bias from the increased frequency of MHW events identified in the last decade (Jacox 2019) and has been done in other MHW studies (Freeland and Ross 2019; Marin et al. 2021; Amaya et al. 2023a). The zero intercept when detrending was at the midpoint of the timeseries so that the mean values averaged over the record did not change.

Using the spatially averaged, detrended surface temperature time series, MHW identification was calculated with the "m-mhw" MATLAB toolbox by Zhao and Marin (2019). The climatology (11-day moving average) and 90^{th} percentile threshold were calculated and then smoothed by a 31-day moving average before identifying MHW events. Additional constraints based on the Hobday et al. (2016) definition include that if there is a two-day gap between two five-day minimum periods in a MHW state, those two periods are classified as part of a single MHW event. A total of 84 discrete MHW events evenly distributed through time were identified from 1986 to 2021 using this method on the detrended surface temperature time series (Figure 1b). The MHW onset and decline phases for each event were then identified, with the onset phase being defined as the period from the MHW start date to, and including, the maximum intensity day and the decline phase being from the maximum intensity day to the end date of the MHW event. To

examine the surface and subsurface conditions before and after MHW events, the 90 days (the window in which mean SST anomalies were greater than zero) preceding and following each MHW event were also identified, excluding MHW days within that period.

2.4 Subsurface Analysis

The *in-situ* subsurface temperature, salinity, and DO profiles were linearly interpolated with depth at intervals of 0, 0.5, and 1 m for the surface values and then every meter to 1 m above the bottom. Density was calculated before the vertical interpolation of profiles from the subsurface temperature and salinity data with a reference pressure of zero using the Gibb Seawater Oceanographic Toolbox (TEOS-10) for MATLAB (McDougall and Barker 2011).

The SML depth (MLD) was calculated using the Irby et al. (2016) definition: the depth where 10% of the total change in density across the vertical extent of the water column occurs over one meter. Additionally, the upper first meter of the water column was not considered in the calculation as recommended by the CBP (USEPA 2004). However, Irby et al. (2016) did not use CBP stations in the more vertically well-mixed upper Bay, near the mouth of the Susquehanna River (here the Susquehanna River mouth is defined as the first CBP station). A definition for a well-mixed water column — the total density difference over depth of the water column scaled by the total depth being less than or equal to 0.1 kg m^{-4} (the CBP threshold for the MLD) — was included in the calculation of the MLD to avoid identifying a MLD for relatively weak water column stratification.

To obtain daily climatologies and anomalies from the monthly/bi-monthly profiles, subsurface temperature, salinity, and DO data at each station at every depth were linearly interpolated through time at a daily resolution. Before interpolation, the linear temporal trends in

the time series at each spatial point were removed, consistent with the surface temperature time series used in the MHW calculation and again to remove the effect of any long-term increases in temperature or decreases in DO; gaps of two months or longer were not interpolated. Following this, at all depths and stations, a daily mean climatology was constructed from the interpolated values and anomalies were calculated by subtracting the subsurface temperature, salinity, and DO samples from the respective daily climatology at each spatial point. Other methods for estimating climatologies and anomalies, such as harmonic analysis and monthly averages, were also tested, but the results generated were not sensitive to method changes. Additionally, the hypoxic layer depth was calculated from the detrended DO profiles using a threshold of 2 mg L^{-1}, used in other studies (e.g., Murphy et al. 2011; Irby et al. 2018; Ni et al. 2019).

The CBP profile sampling dates were then cross-referenced with the dates of MHWs identified by the spatially averaged surface temperature time series to classify profiles taken before, during, or after MHW events. This resulted in identifying approximately 760 "MHW profiles" (e.g., profiles that occurred during a surface MHW event), or 30 to 40 profiles per station (Figure 1g), with 36.9% of MHW events partially represented (31/84 events; having at least one station captured) and 23.8% of MHW events (20/84 events) fully represented by all 21 stations along the CB main stem (Figure 1d). Note that the profiling transects across the CB occurred over timescales of approximately three to five days and did not always line up with the entire MHW event. During the spring, late fall, and winter months (February, March, May, November and December) 0-3 profiles per station were available, while during the summer and early fall months (June, July, August, September, and October) 3-8 profiles per station were available (Appendix 1). Additionally, a total of 31 MHW profiles were sampled in wet years and 21 profiles in dry years (Figure 1e). Though only 6.5% of MHW profiles (51/760) were sampled in wet or dry

years—59.3% of the MHW profiles identified in May (19/32) were sampled in wet years and 44.4% of MHW profiles in December were sampled (16/36) in dry years.

To eliminate the impact of wet years and dry years, since there are fewer MHW profiles in the tails of the annual discharge distribution (Figure 1c), the linear relationships between the salinity anomalies, and the temperature and DO anomalies, respectively, were removed using linear regression analysis, and has been done in previous work (Murphy et al. 2022). Removing the relationship between salinity and DO is especially important since the primary driver of variability in DO is Susquehanna River discharge which modulates salinity (Li et al. 2016). This prevented a small number of profiles sampled during anomalous discharge years from biasing the MHW profile analysis.

Finally, monthly subsurface panels (e.g., Figures 3 & 4, See section *3.2 Seasonal Patterns of Subsurface Anomalies*) were smoothed with a 3-month moving average. This was done to reduce noise in spring, fall, and winter months with only a few (0-3) profiles per station available (Appendix 1). All twelve panels were smoothed, including the months (June to October) with more adequate amounts of data (3-8 profiles per station), to remain consistent (Appendix 1). Additionally, the synoptic plots (e.g., Figures 6 & 7, See section *3.3 Synoptic Subsurface Anomalies*) were smoothed with a 3-day moving average, to reduce the noise due to low data availability on certain days (Appendix 2 & 3).

2.5 Surface Mixed Layer Heat Budget

To understand the dynamics and drivers of MHWs, a SML heat budget analysis can be performed (Moisan and Niiler 1998; Oliver et al. 2021; Schlegel et al. 2021) to characterize the sources and sinks of heat in the SML during MHW events. This model can be described as:

$$\frac{\partial T_{SML}}{\partial t} = \frac{Q_{net}}{\rho c_p H} - u_{SML} \cdot \nabla_h T_{SML} + R \quad (1)$$

where the left-hand term represents the change in temperature of the SML (T_{SML}) through time (t) and the right-hand terms represent the air-sea heat flux, horizontal advection (u_{SML}) across the thermal gradient ($\nabla_h T_{SML}$) in the SML, and residual terms (R; i.e. vertical and horizontal mixing and entrainment terms). The air-sea heat flux term is composed of the net downward heat flux (Q_{net}), which is a summation of Q_{LR}, Q_{SR}, Q_{SH}, and Q_{LH}, scaled by the water density (ρ), specific heat content of the water (c_p), and the seasonally varying MLD (H).

While the present data do not allow for the calculation of the advective nor residual terms of the SML heat budget (eq. 1), they do allow for the inspection of the role of air-sea heat flux contribution to temperature changes in the SML (e.g., Schlegel et al. 2021):

$$\frac{\partial T_{Qnet}}{\partial t} = \frac{Q_{SR}+Q_{LR}+Q_{SH}+Q_{LH}}{\rho c_p H} \quad (2)$$

and examine if the primary driver of the onset and decline of MHWs in the CB was air-sea heat flux as suggested by Mazzini and Pianca (2022). Following Schlegel et al. (2021), I calculated the temperature change during each MHW phase (onset and decline) due to Q_{net} and each individual heat flux term (Q_x; x = LR, SR, SH, LH) in the SML by taking the time integral of eq. (2):

$$T_{Qx}(t) = \int_{t0}^{t} \frac{Q_x(S)}{\rho c_p H(S)} ds \quad (3)$$

where t_0 and t are the beginning and end of each phase (onset or decline) of the MHW respectively. However, in our analysis, spatially averaged Q_{net}, Q_x, and H were used in eq. (3), which resulted in a simplified 1-D version of the SML heat budget model consistent with the single spatially averaged time series used to represent the surface temperatures of the CB. To obtain anomalies of T_{Qx} comparable to the SST anomalies (SSTa), anomalies of Q_x/H were calculated from a daily

climatology and then applied to eq. (3) (Schlegel et al. 2021). Additionally, the constant values of 4090 J kg^{-1} K^{-1} and 1009.9 kg m^{-3} (calculated mean CB density) were used for c_p and ρ.

In this simplified model, eq. (3), a temperature anomaly definition of *H*, instead of a density definition (described above), of the MLD was used. *H* was defined as the depth at which 90% of the total range in temperature anomalies across the vertical extent of the water column during a MHW event was captured. This temperature anomaly definition of *H* was used to prevent a misidentification of a MLD during the winter season, which is presumably thermally homogenous (Appendix 4). CBP sampling is restricted to days without inclement weather (CBP 2017), which likely biases profiles to a more stratified representation of CB (e.g., more vertical mixing expected during inclement weather) and in turn biases the heat budget analysis (Elzahaby et al. 2022). A sensitivity analysis of the 90% threshold for the identification of *H* indicated that a change of ±5% to the threshold did not substantially change the number of events identified as being driven by air-estuary heat flux. During the onset, there was an ~2% decrease in events identified (42/43) with a 5% threshold increase, and an ~5% increase in events identified (45/43) with a 5% threshold decrease, while there was no change during the decline phase. Finally, due to limitations of the CBP data, a seasonal (monthly) median spatially aggregated climatology of *H* was calculated from the MHW profile, a similar method used in other studies (Ross and Stock 2022; Appendix 5).

To determine relative contribution of atmospheric forcing during the onset or decline of MHW events, the ratios of T_{Qnet} to SSTa and of T_{Qx} to T_{Qnet} were calculated similarly to Schlegel et al. (2021). The ratio of T_{Qnet} to SSTa indicates the proportion of change in SSTa due to T_{Qnet}, where a ratio greater than 0.5 indicates that heat flux is the leading driver of a MHW phase. Similarly, the ratio of T_{Qx} to T_{Qnet} indicates which component of the air-sea heat flux is the primary contributor to net atmospheric heat flux, and was calculated during atmospherically driven events.

3. Results

3.1 Spatial Patterns of Subsurface Anomalies

During MHW events, on average, warmer temperatures were seen across the entire CB, with anomalies ranging between 0.5-3°C (Figure 2a). The greatest temperature anomalies (~3°C) were present above the MLD in the UB, and lowest anomalies (~0.5°C) were present below the MLD in the UC. Apart from the UB and UC surface layers, which were ~0.5°C warmer than the LC and LB, the surface temperature anomalies were nearly horizontally uniform across the entire Bay. In general, the MLD was several meters shallower in the UC and LC during MHW events compared to the annually averaged climatological MLD ($MLD_{\mu\ clim}$), while it was at approximately the same depth in the UB and LB. All temperature anomalies greater than 2.5°C were found above the MLD and all temperature anomalies greater than 1.5°C were found below the MLD in the LB and above the Rappahannock shoals (see Figure 1a) in the LC. Otherwise, much of the deep channel had ~1°C temperature anomalies. Additionally, the temperature anomalies in the UB were generally vertically homogeneous while the rest of the CB was stratified to some degree. From this homogenous region in the UB to the UC, there was a sharp vertical change (~2.5°C across water column) in the magnitude of temperature anomalies. This vertical range in anomalies was present across much of the Bay. The greatest variation in temperature anomalies was seen near the mouth of the Susquehanna River ($\sigma = \pm 1.5$°C, where σ is the standard deviation), in the LB near the mouth of the CB ($\sigma = \pm 2$-2.5°C), and at the bottom of parts of the UC and LC ($\sigma = \pm 2$-3°C), while the smallest variations were seen above MLD and at the bottom of UB and LB ($\sigma = \pm 0$-0.5°C; Figure 2b). Otherwise, there was a generally consistent standard deviation of ~1°C across most of the Bay.

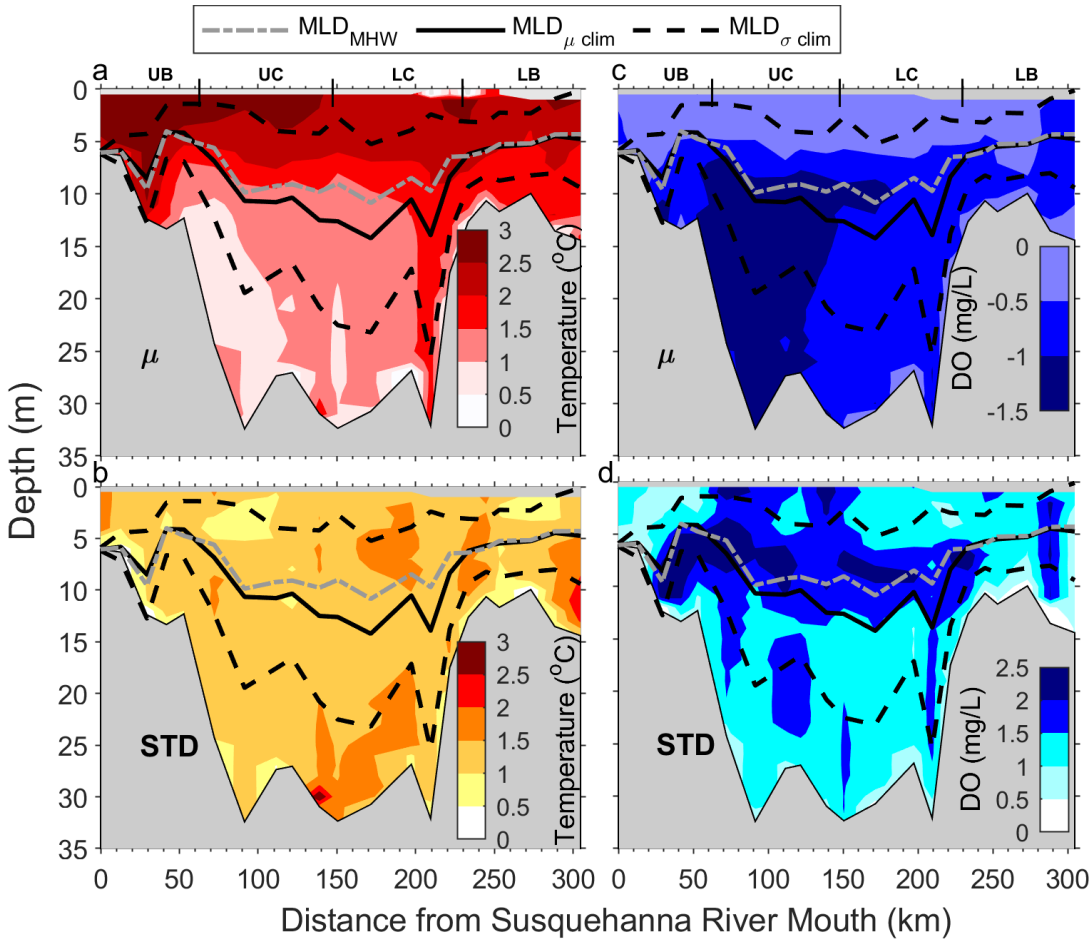

Figure 2. Mean Temperature and Dissolved Oxygen Anomalies During Surface Marine Heatwave (MHW) Events. Each point is the monthly weighted annual average and standard deviation of temperature (a and b), DO (c and d), and MHW mixed layer depth (MLD_{MHW}; grey dotted dashed line) and the annually averaged climatological MLD ($MLD_{\mu\ clim}$; black solid line) and standard deviation ($MLD_{\sigma\ clim}$; black dashed line). Regions of the Chesapeake Bay—Upper Bay (UB), Upper Channel (UC), Lower Channel (LC), Lower Bay (LB)—are indicated (a and c).

During surface MHW events, DO levels were generally lower (e.g., negative anomaly) by at least 0.5 mg L^{-1} across the Bay (Figure 2c). Yet, the greatest decreases in DO (1-1.5 mg L^{-1}) were observed primarily in the deep channel of the Bay below the MLD with the effect being greatest in the UC (negative DO anomalies of ~1.5 mg L^{-1}). Additionally, these anomalies were generally observed at or below the MLD across the deep channel. This region in the middle of the water column was also where the greatest variability of DO (σ = ±1.5-2 mg L^{-1}) occurred in addition to the surface waters of the UC (Figure 2d). DO variability was lowest along the bottom

of the main stem of the Bay ($\sigma = \pm 0.5$ mg L^{-1}), where the most negative anomalies were observed. Otherwise, there was a generally consistent standard deviation of ~1 mg L^{-1} across the Bay.

3.2 Seasonal Patterns of Subsurface Anomalies

Hydrographic

Two contrasting seasonal patterns of temperature anomalies were evident during MHW events in the CB main stem: a stratified spring-summer season and a homogeneous fall-winter season (Figure 3). During the stratified season (April to August) positive temperature anomalies of up to 4℃ were only present in the upper 10-15m of the water column, with the greatest anomalies present in April and May. However, these large anomalies (3-4℃) in April and May (Figure 3) did not push temperatures in these months (~16℃ and 21℃ respectively) to mean surface summertime temperatures (28℃; Appendix 4). Meanwhile, the smaller anomalies in the summer (~1℃; Figure 3) pushed temperatures towards 30℃ (Appendix 4). Additionally, anomalies greater than 1℃ were absent in the deep channel of the main stem, and the 1℃-anomaly contour did not extend below the MLD. In contrast, during the homogeneous season, from October to February, temperature anomalies ranged from 0-3 ℃ and anomalies greater than 1℃ were found throughout the water column, including the deep channel. Fall-winter anomalies in the deep channel were generally 1-2℃ greater than the spring-summer anomalies. However, these contrasting patterns were primarily present in the deep channel of the main stem, while the seasonal and spatial patterns in the shallow UB and LB differed.

Generally, surface monthly temperature anomalies were horizontally homogeneous across the entire length of the main stem, but there were variations with depth especially in the shallow regions (Figure 3). In the UB, the MHW anomalies were vertically homogeneous year-round,

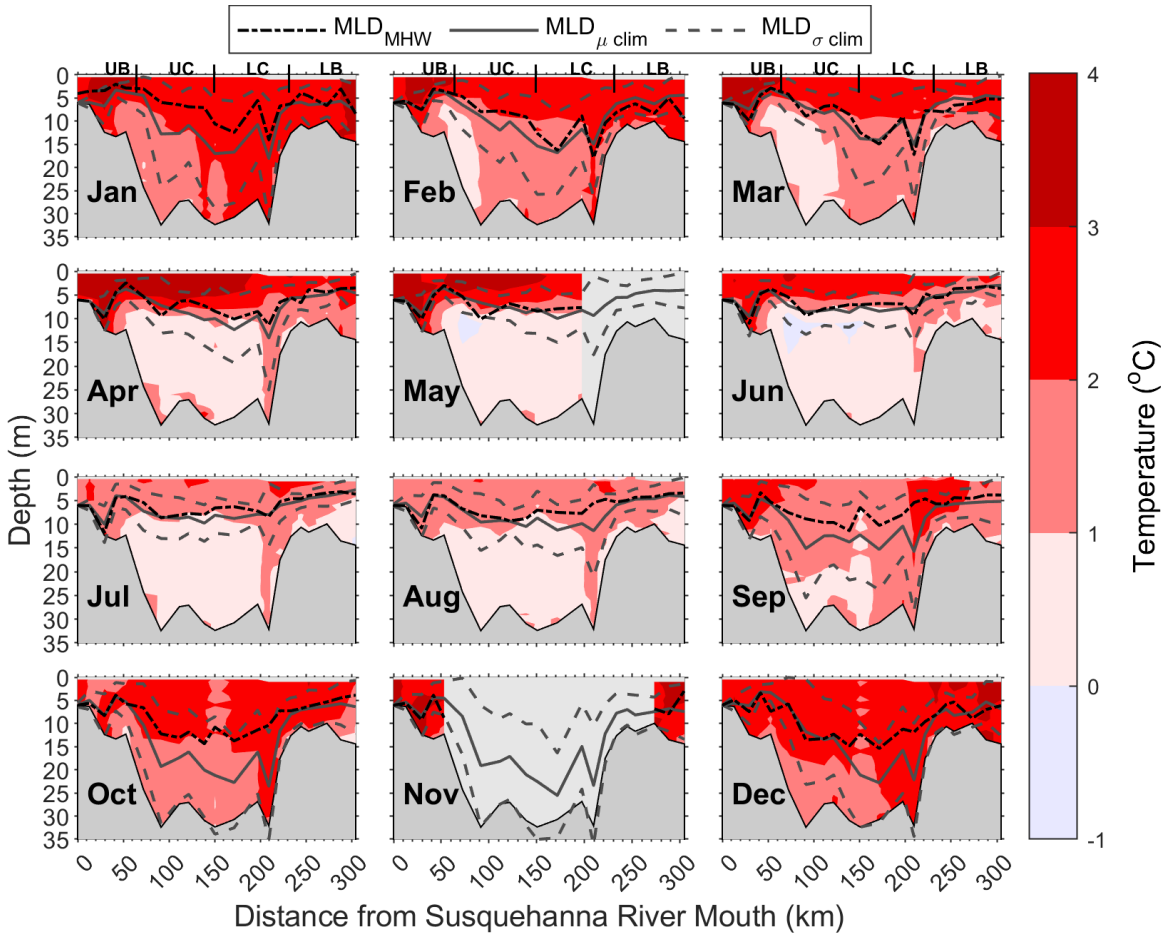

Figure 3. Mean Monthly Temperature Anomalies During Surface Marine Heatwave (MHW) Events. Each point is the monthly average of all available MHW temperature anomaly profiles. The average monthly MHW MLD (MLD_{MHW}; black dotted dashed line) is also plotted for each station in addition to the climatological average MLD ($MLD_{\mu\ clim}$; grey solid line) with one standard deviation ($MLD_{\sigma\ clim}$; grey dashed line). Missing data in May and November are indicated by the light grey. Regions of the Chesapeake Bay are indicated as in Figure 2.

while in LB, down estuary of the Rappahannock shoals (see Figure 1a), there was a muted seasonal pattern consistent with the deep channel (e.g., homogeneous anomalies in the fall-winter and stratified anomalies in the spring-summer; Figure 3). Additionally, in the deep channel from February to April, the 1°C-temperature anomaly contour moved down the deep channel from the UC to the LC until the stratified regime formed across the entire channel in the spring months. The exception to these patterns being at the Rappahannock shoals where warm temperature anomalies were present at depth during MHW events year-round.

It is important to note, however, there were seasonal biases in the availability of MHW profiles, with the number of profiles per station per month ranging from 0-8 profiles (Appendix 1). The fewest profiles (0-3 profiles per station) were available from the late fall through the spring, while the most profiles (3-8 profiles per station) were available from the summer to the early fall. Nonetheless, the seasonal variations and trends discussed above are fairly consistent within a given season, indicating that the major conclusions on seasonal changes and structure are likely not affected by the data availability.

The seasonal variation of vertical structure of temperature anomalies during MHW events was generally consistent with the seasonal cycle of MLD (Figure 3). In the winter and fall months (October to February) the climatological average MLD ($MLD_{\mu\ clim}$) in the channel was deeper (~15 m depth), with greater variance, as indicated by a larger $MLD_{\mu\ clim}$ standard deviation ($\sigma = \pm$ 6.1 m; $MLD_{\sigma\ clim}$; Figure 3), which corresponded to reduced seasonal stratification (Appendix 6). However, in the spring and summer the $MLD_{\mu\ clim}$ in the channel was shallower (~7 m depth), with less variance, as indicated by a smaller $MLD_{\sigma\ clim}$ ($\sigma = \pm$3.4 m; Figure 3), which corresponds to increased seasonal stratification (Appendix 6). During MHWs the MLD (MLD_{MHW}) shoaled by an average of 2.0 m across most of the deep channel (Figure 2). This shoaling was generally greater in the fall-winter season (~3 m) than in the summer (~1 m), but the MLD_{MHW} did not exceed more than one standard deviation beyond that of the $MLD_{\mu\ clim}$ in either season. Additionally, in the late winter through the spring (February to May) there was a progressive shoaling of $MLD_{\mu\ clim}$ and MLD_{MHW} in the deep channel (Figure 3) that corresponded to increased stratification in the Bay (Appendix 6). This shoaling also corresponded with a spring movement of the MHW temperature 1°C anomaly contour from the UC to the LC.

Dissolved Oxygen

In general, during MHWs there was a small (<1 mg L^{-1}) decrease (e.g., negative anomaly) of DO across the entire main stem and during all months (Figure 4). From July to September there were minimal decreases (0-1 mg L^{-1}) in DO throughout most of the water column. Varying levels of greater negative DO anomalies (~1-4 mg L^{-1}) were observed from late fall through the spring. During the winter (December to February), low DO anomalies (negative anomalies of ~1-3 mg L^{-1}) were focused across the deep channel and mostly below the identified MLD. In the spring months (March to May), the largest negative DO anomalies (~2-4 mg L^{-1}) were observed throughout the water column below the MLD in the UC, as well as just below the MLD in the LC (~2 mg L^{-1}). While the pattern in June was similar, 1 mg L^{-1} negative DO anomalies were mostly observed 5-10 m below the MLD. The largest negative DO anomalies (4 mg L^{-1}) were captured in the spring season. However, from April to August slightly positive anomalies (0-2 mg L^{-1}) were also observed in the surface waters in the channel regions (Figure 4), which are associated with elevated levels of chlorophyll, indicating elevated rates of photosynthesis (Appendix 7).

In most instances, from April until October, these lower DO levels were associated with an expansion of the hypoxic region of the Bay (Figure 4). Starting in April in the UC and persisting across the Bay through the hypoxic season (May to September; Appendix 8) to October, the hypoxic contour was raised above climatological levels (Figure 4). During April in the UC, 1-2 mg L^{-1} decreases in DO resulted in DO reductions to borderline hypoxic (~2-3 mg L^{-1}) levels in the bottom waters, while in the middle water column a 1-3 mg L^{-1} DO reduction resulted in ~5-9

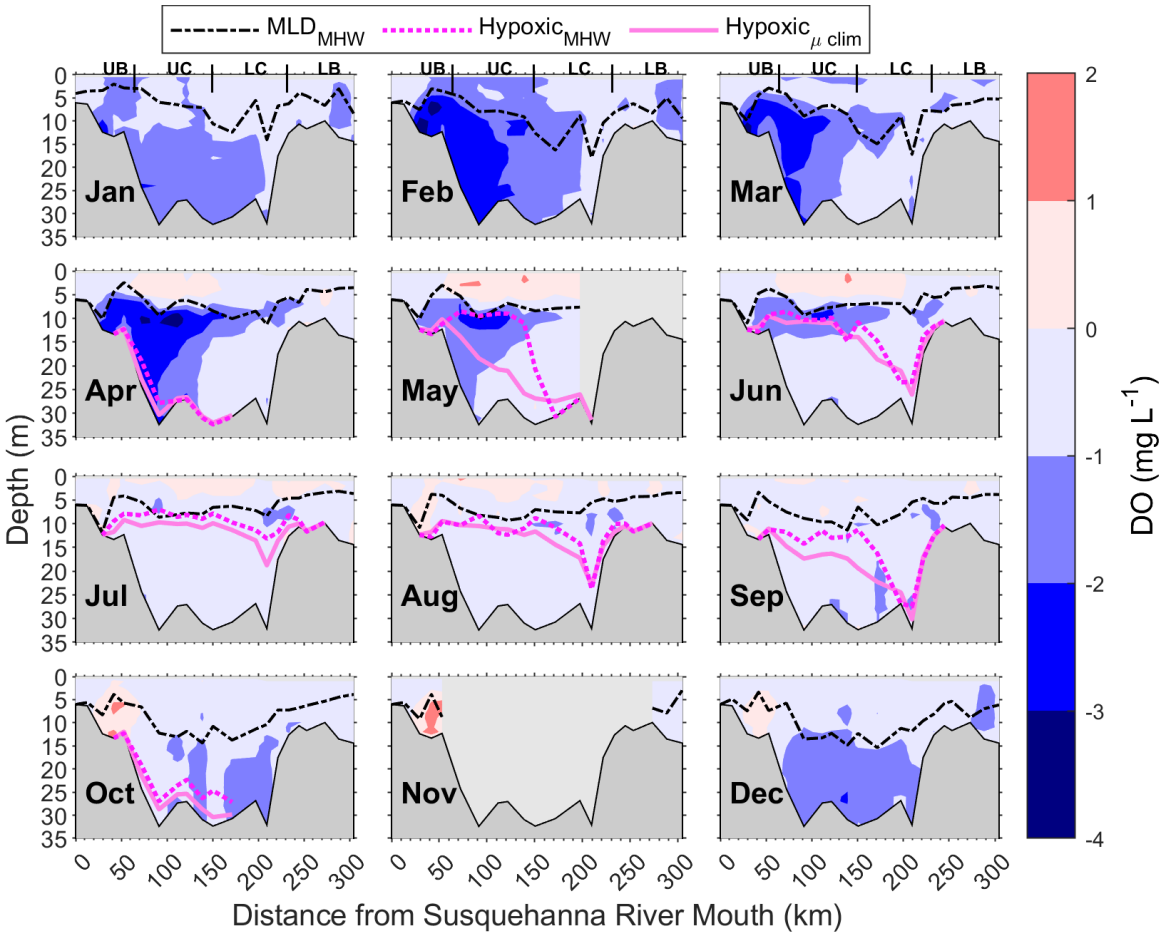

Figure 4. Mean Monthly Dissolved Oxygen (DO) Anomalies During Surface Marine Heatwave (MHW) Events. Each point is the monthly average of all available MHW DO anomaly profiles. The climatological ($Hypoxic_{\mu\ clim}$; magenta solid line) and MHW ($Hypoxic_{MHW}$; magenta dotted line) hypoxic contour (2 mg/L) are plotted along the top of the hypoxic zone for each station when hypoxia is present. Regions of the Chesapeake Bay and sample locations are indicated as in Figure 2. Missing data and the MHW mixed layer depth are indicated as in Figure 3.

mg L^{-1} DO concentrations (Figure 4; Appendix 8). Meanwhile in May, similar reductions in DO caused much of the UB to become hypoxic (Figure 4). In July, when seasonal hypoxia reached its farthest extent, until October, small decreases in DO (< 1 mg L^{-1}) were associated with expansions of the hypoxic zone into regions that were borderline hypoxic (2-3 mg L^{-1}; Figure 4; Appendix 8). However, unlike in April and May, the large decreases in DO (1-3 mg L^{-1}) observed during the winter and early spring, were not associated with hypoxia (Figure 4), because the Bay was well oxygenated at that time, with DO levels being only reduced to 6-10 mg L^{-1}, well above hypoxic levels (Appendix 8).

A correlation analysis at every station and depth indicated that there were statistically significant positive and negative relationships between temperature anomalies and DO anomalies during MHW events (Figure 5; Thomson and Emery 2014). Specifically, negative correlations were present in the UB near the mouth of the Susquehanna River throughout the water column (R = -0.8 to -0.4), in the bottom waters of the UC (R = -1 to -0.4), and in the bottom waters of the LB near the mouth of the CB estuary (R = -0.8 to -0.4; Figure 5a). In the UB and LB, while correlations were statistically significant, slopes from regression analysis between DO and temperature anomalies were small, representing linear decreases between 0.2 to 0.4 mg L^{-1} and 0 to 0.4 mg L^{-1} of DO per a 1°C of warming, respectively (Figure 5b). However, in the bottom waters of the UC in the regions of statistically significant correlation, DO decreased anywhere from 0.4 to 1.6 mg L^{-1} of DO per a 1°C increase (Figure 5b) with ~20% of this decrease in DO resulting from decreases in DO solubility due to elevated temperatures, suggesting other mechanisms of oxygen drawdown

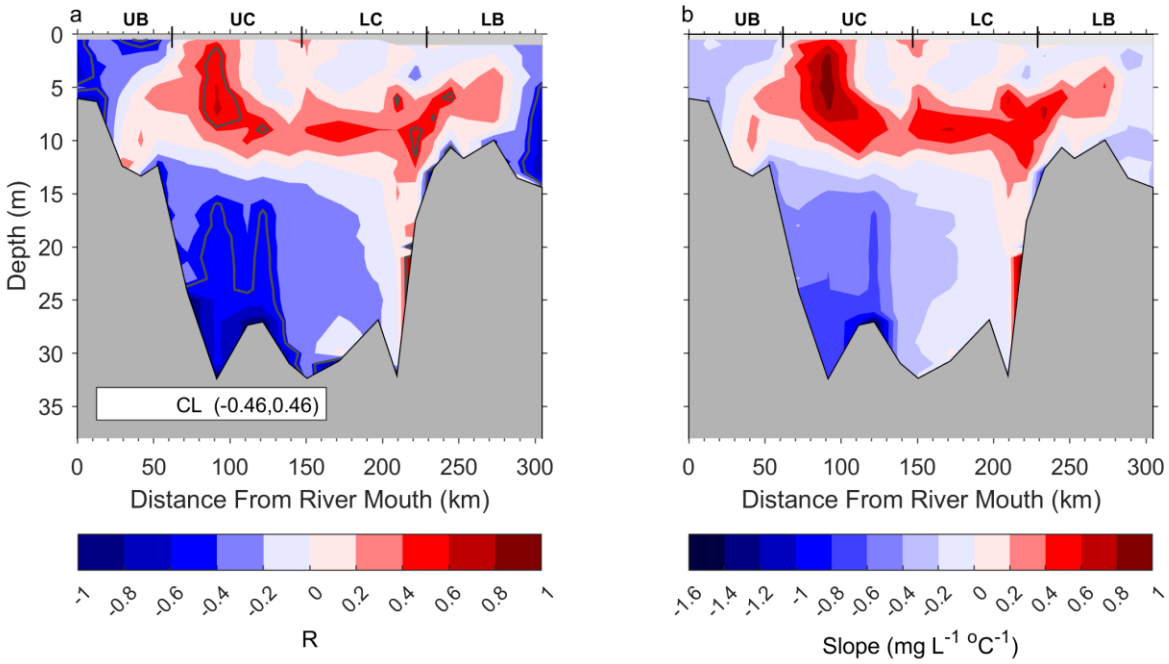

Figure 5. Linear Relationship of Dissolved Oxygen (DO) Anomalies to Temperature Anomalies. The correlation (a) and slope (b) were calculated based on the available subsurface temperature and DO data at each grid point. The correlations within the grey contours in *a* indicate a confidence level of 0.95. Regions of the Chesapeake Bay are indicated as in Figure 2.

(Appendix 9). Positive correlations between temperature and DO anomalies were present in the middle of the water column and near the surface in the UC (R = 0.4-0.6) and LC near the Rappahannock shoals (R = 0.4; see Figure 1a; Figure 5a). In the UC, increases of 0.4 to 1 mg L^{-1} per 1℃ of warming occurred (Figure 5b). These positive correlations were not due to changes in solubility during MHW events, but were presumably associated with increased photosynthesis, highlighted by elevated chlorophyll-a levels in this region of the Bay during MHWs (Appendix 7, 9). Increased temperatures during MHW events were therefore linked to both increases and decreases in DO levels depending on the region.

3.3 Synoptic Patterns of Subsurface Anomalies

Prior to MHW events during the stratified season (April through August), surface mean temperature anomalies (spatially-averaged and including the entire 25-year time series) were elevated by approximately 0.5℃ for 62 days, which began to increase from that baseline 8-9 days before events (Figure 6a) and were elevated by 0.5℃ for 70 days after events after a 2-day decline (Figure 6b). Consistent positive surface temperature anomalies (μ = 1-1.5℃; $\mu-\sigma$ >0℃) were present 4 days before events (Figure 6a) with subsurface anomalies (>0.5℃) present 4-5 days before events (Figure 6c, e, g, i), and up to 18 days in the LC (Figure 6g). After event initiation, subsurface positive anomalies lasted for 4-10 days (LB and UC; Figure 6j, f) and only for 2 days in the surface (Figure 6b). Subsurface temperature anomalies were generally stratified, except in the UB where they were homogeneous. Additionally, the MLD shoaled 2-5 m from a stable position over a 2-5-day period before MHWs and then returned to its relative baseline 2-4 days following these events (Figure 6c-j).

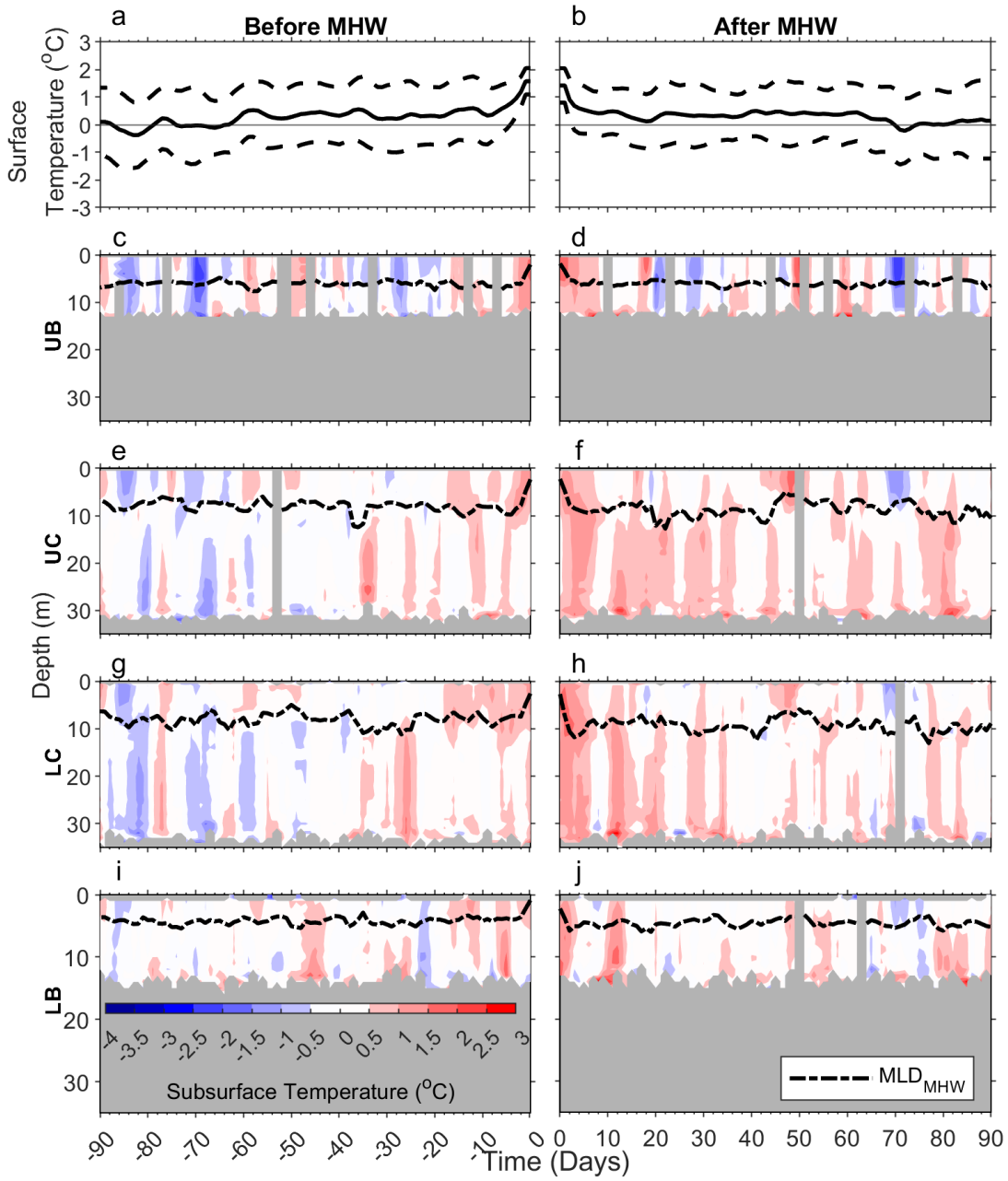

Figure 6. Surface and Subsurface Temperatures Before and After Marine Heatwave (MHW) Events During the Stratified Season (April-August). The daily average (black solid line) and standard deviation (black dashed line) of the spatially averaged surface temperature time series before (a) and after (b) MHW events, with a grey reference line plotted at zero. Each subsurface profile is the average of all available profiles taken each day before (c, e, g, i) and after MHW events (d, f, h, j) from April to August across the entire time series in each region of the Bay: Upper Bay (UB; c, d), Upper Channel (UC; e, f), Lower Channel (LC; g, h), Lower Bay (LB; i, j). The grey areas indicate missing data, or the bottom, and the dotted dashed line indicates the mean daily mixed layer depth before and after MHW events (MLD_{MHW}).

During the homogeneous season (October through February), positive mean surface temperature anomalies were present and increasing for 26 days before MHWs (Figure 7a) and fell back to 0℃ 18 days after the event (Figure 7b). Consistent positive surface temperature anomalies (μ = 1-2℃; μ-σ >0℃) were present for 5 days prior to MHWs (Figure 7a), with homogeneous subsurface anomalies, ranging from 0.5-2℃, present in the channel (Figure 7e, g) and LB (Figure 7i) up to 10 days before MHW events. After MHWs, surface anomalies lasted for 7 days (Figure 7b) with homogeneous subsurface anomalies greater than 0.5℃ present for 10-20 days across the entire Bay (Figure 7d, f, h, j). Though the MLD was more variable than the stratified season, 5-15 m shoaling of the MLD was present for ~5 days before MHW events and relaxed over several days following MHW events (Figure 7c-j).

It is important to note that during the stratified season (Appendix 2), there was an average of 8.0 samples per depth per day with a range of 0 to 34 samples collected before MHW events, and 6.8 samples per day per depth with a range of 0 to 35 samples collected after MHW events. However, during the homogenous season (Appendix 3), there was an average of only 2.1 samples per depth per day with a range of 0 to 18 samples collected before MHW events, and 2.7 samples per depth per day with a range of 0 to 22 samples collected after MHW events. Additionally, this analysis was not performed for DO anomalies because there were sizable horizontal gradients in DO, which resulted in a large amount of noise when averaging random profiles to construct a synoptic time series, unlike temperature anomalies, which showed only weak or absent horizontal gradients.

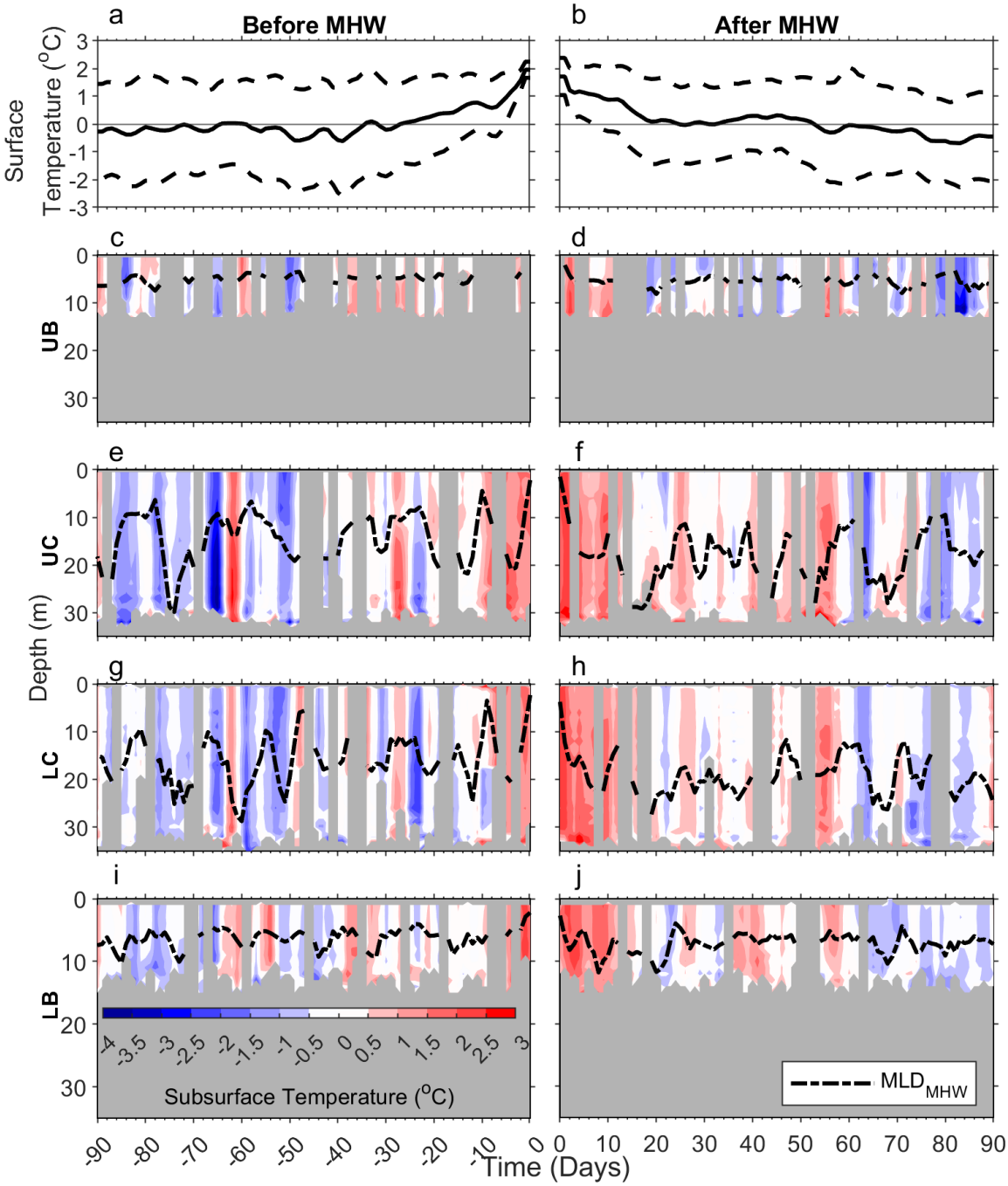

Figure 7. Surface and Subsurface Temperatures Before and After Marine Heatwave (MHW) Events During the Homogenous Season (October-February). Data was averaged the same way as Figure 6, except for the averaging period being the months of October to February instead of April to August. Additionally, regions, missing data, and the mixed layer depth are indicated in the same way as Figure 6.

3.4 Heat Budget

Atmospheric forcing was a leading driver of MHWs in the CB during both their onset and decline phases (Figure 8). Surface heat fluxes contributed to the onset of every identified MHW and the majority (72/84) of their declines ($\Delta T_{Qnet}/\Delta SSTa > 0$), with only 14.3% (12/84) of events not contributing to the decline ($\Delta T_{Qnet}/\Delta SSTa \leq 0$; Figure 8b). The median proportion of change in ΔSSTa in the onset and decline phase of MHWs, 0.52 and 0.41 respectively, suggested a sizable and consistent contribution of surface heat fluxes during both the onset and decline of MHWs

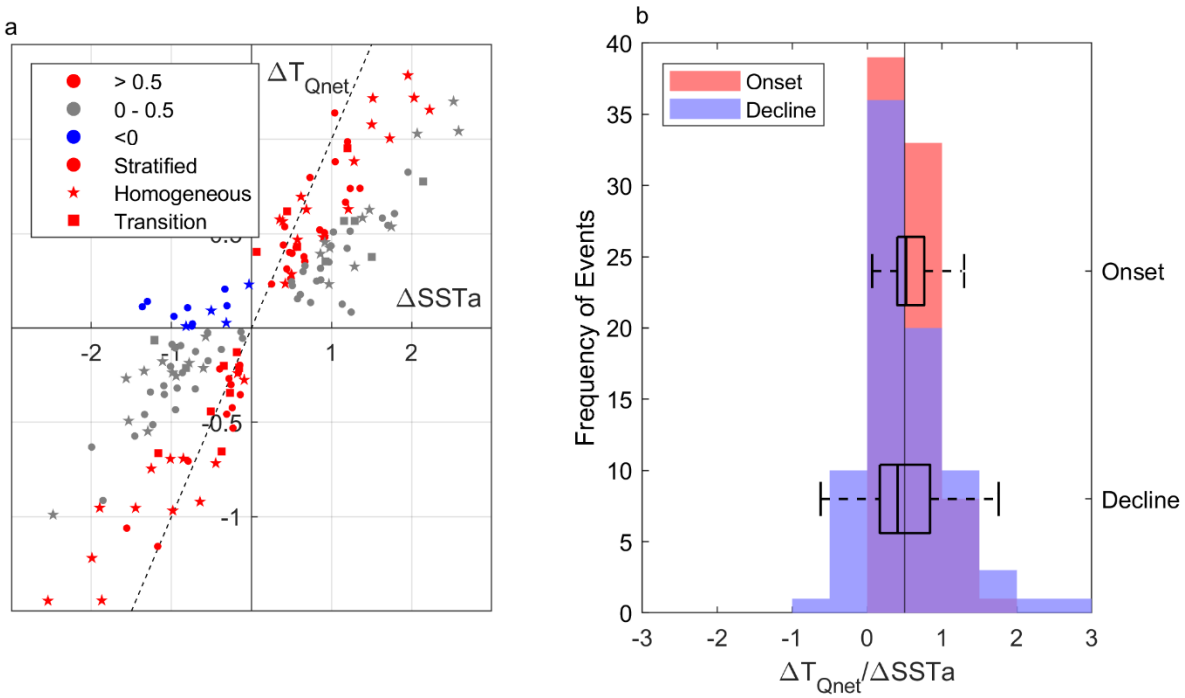

Figure 8. Contribution of the Change in T_{Qnet} to the Change in Surface Temperature Anomalies. (a) The relationship of the change in the spatially averaged temperature time series anomalies (ΔSSTa) and the change in temperature anomaly due to net heat flux (ΔT_{Qnet}) during the onset (ΔSSTa>0) and decline (ΔSSTa<0) phases of each MHW event, where greater than half (red), zero to half (grey), and less than zero (blue) of the change in ΔSSTa attributed to the change in ΔT_{Qnet} are indicated. Points in line with the grey dashed line indicate a one-to-one relationship between ΔT_{Qnet} and ΔSSTa, while points along the x-axis indicate little relationship between ΔT_{Qnet} and ΔSSTa. (b) The distribution of the proportions of ΔT_{Qnet} and ΔSSTa for each event for the onset (red) and decline (blue) phases. The middle vertical line of the boxplots indicates the median proportion of change, the left and right vertical lines indicating the interquartile range (25th-75th percentile) and the whiskers indicate the range of data that falls within 1.5 times the interquartile range. All outliers have been excluded from the plot. Negative proportions of ΔT_{Qnet} and ΔSSTa imply that the change in ΔT_{Qnet} is acting against the change in ΔSSTa during a given phase. For reference, the 0.5 value (vertical grey line) is indicated to show if ΔT_{Qnet} drives ΔSSTa in each phase.

(Figure 8b). Over half, 51.2% (43/84), of events had air-sea heat flux as the leading driver ($\Delta T_{Qnet}/\Delta SSTa > 0.5$) during the onset phase of MHW events, while only 42.9% (36/84) of MHWs had air-sea heat flux as the leading driver ($\Delta T_{Qnet}/\Delta SSTa > 0.5$) during their decline.

Additionally, there were large seasonal variations in the dominance of atmospheric heat flux. During the homogenous season, 58.6% (15/29) of event onsets and 37.9% (11/29) of event declines were atmospherically driven, while during the stratified season 51.2% (22/43) of onsets and 31.8% (14/44) of declines were atmospherically driven. Most declines (22/44) during the stratified season were only partially driven by atmospheric fluxes ($0 < \Delta T_{Qnet}/\Delta SSTa \leq 0.5$ &), indicating that other processes drive the decline of surface MHWs during the stratified season. The greatest changes in ΔT_{Qnet} and ΔSSTa were seen in the onsets and declines of events during the homogenous season (Figure 8a).

Of the MHW events primarily driven by surface heat fluxes, Q_{LH} flux had the overall greatest median proportion of the total air-estuary heat flux during both the onset and decline phases, 0.50 and 0.58 respectively, with Q_{SR} flux being the second largest contributor (0.26 during the onset and 0.21 during the decline; Figure 9). However, Q_{SR} did not consistently contribute to either phase of MHW events. Additionally, Q_{LR} and Q_{SH} equally contributed the least to both the onset or decline of MHWs. However, there were slight seasonal variations in the dominant component of the air-estuary heat flux. During the stratified season, Q_{LH} and Q_{SR} drove the onset (0.35 and 0.41) and decline (0.59 and 0.43) of events. In the homogenous season, Q_{LH} (0.56) and Q_{LR} (0.40) drove the onset of events, whereas during the decline, Q_{LH} (0.45) and Q_{SH} (0.35) were the prominent constituents.

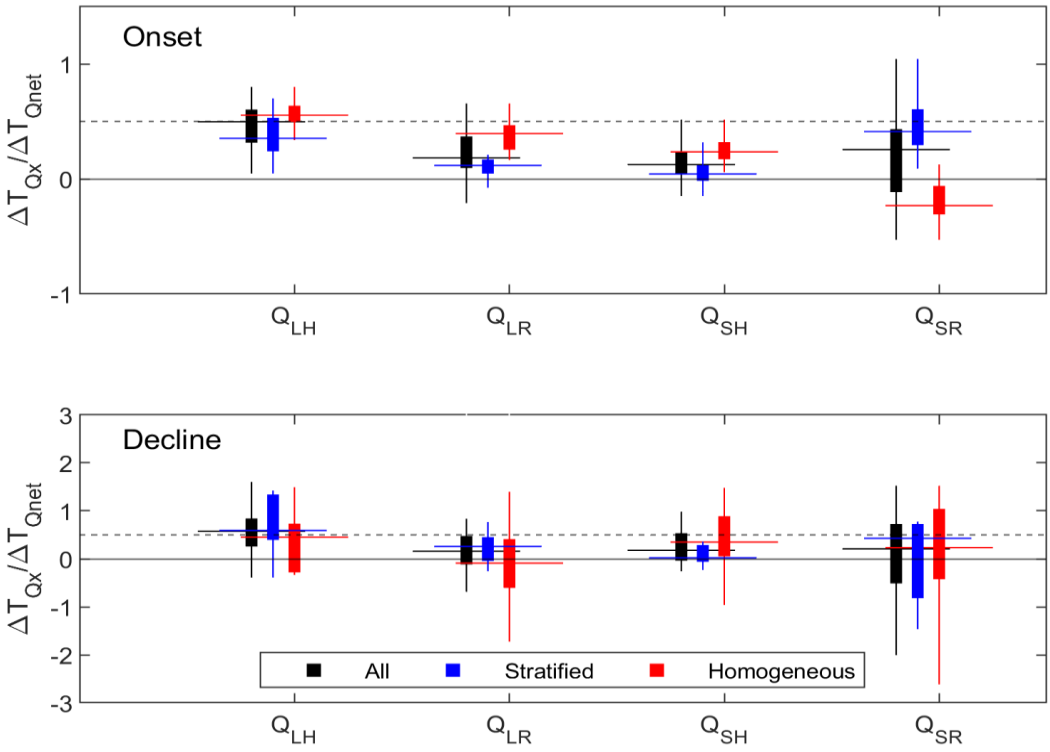

Figure 9. Contribution of the Change of Each Heat Flux Term to the Net Change in Heat Flux during the Onset and Decline Phases. The proportion of ΔT_{Qx} and ΔT_{Qnet} for all marine heatwave (MHW) events (black), the stratified season events (April-August; blue), and the homogenous season (October-February; red). Proportions of ΔT_{Qx} and ΔT_{Qnet} less than zero indicate that a given heat flux term (ΔT_{Qx})—Latent heat (Q_{LH}), Longwave Radiation (Q_{LR}), Sensible Heat (Q_{SH}), or shortwave radiation (Q_{SR})—is inhibiting ΔT_{Qnet} in each MHW phase, while positive values indicate a contribution to ΔT_{Qnet}. The bottom and top edges of the box represent the 25th and 75th percentile, the horizontal line through the boxes indicate the median, and the vertical lines indicate the furthest value from the median within 1.5 times the interquartile range. Reference lines at 0 (solid line) and 0.5 (dashed line) are plotted.

4. Discussion

Previous studies have shown that in the global oceans the greatest temperature anomalies during surface MHW events can occur below the surface (Schaeffer and Roughan 2017; Elzahaby and Schaeffer 2019; Hu et al. 2021; Großelindemann et al. 2022; Amaya et al. 2023a), and that they can endure much longer than those at the surface (Jackson et al. 2018; Freeland and Ross 2019; Amaya et al. 2023a), suggesting that MHWs have the potential to last longer and at a greater

intensity than what is simply indicated by their surface signature. Due to the shallow nature of estuaries, MHWs and their impacts could be further amplified (Oczkowski et al. 2015); yet, to our best knowledge, no prior research has been pursued that targets these extreme events in subsurface estuarine waters. In the present study, I investigated for the first time the spatial and temporal structure of subsurface temperature anomalies associated with surface MHW events and their impact on DO concentrations in the Chesapeake Bay, a large, temperate, partially mixed estuary.

4.1 Temperature Spatiotemporal Variability

In contrast to oceanic subsurface MHW findings, where subsurface temperature anomalies could exceed those at the surface (Schaeffer and Roughan 2017; Elzahaby and Schaeffer 2019; Hu et al. 2021; Großelindemann et al. 2022; Amaya et al. 2023a), I found the greatest temperature anomalies in CB were invariably found in the near-surface (reaching up to 4℃), with decreasing intensities at depth that varied seasonally. I identified two contrasting subsurface seasonal patterns of temperature anomalies in the CB in response to surface MHWs: a thermally stratified spring-summer season and a thermally homogenous fall-winter season (Figure 3). During the stratified season, notable positive temperature anomalies (1-4℃) were only observed in the upper water column (upper 10-15m) and absent below the MLD in the channel. This thermally stratified season coincided with the season of strong density stratification and a shallower and less variable MLD. In contrast, during the homogenous season, which corresponded with a weak density stratification and a deeper and more variable MLD, temperature anomalies (1-3℃) were present at all depths. Additionally, these general patterns were present even if the surface temperature time series used for MHW detection was not detrended. This indicates that these are robust patterns which are

persistently present during extreme temperatures in the Bay, since detrending the data changed which days (and temperature profiles) were identified as MHWs.

The seasonal patterns discussed above represent two distinct subsurface regimes associated with surface MHWs, with stratification likely controlling the subsurface temperature response. These patterns are largely consistent with a simple one-dimensional response to heat, sourced primarily through the air-estuary interface (Figure 8), and downward heat transport and diffusion controlled by seasonally variable stratification and mixing. In the CB, the seasonal cycle of stratification (Appendix 6) is primarily driven by the seasonal cycle of fresh water input from Susquehanna River discharge (Li et al. 2016), which consequently affects the vertical temperature distribution. Stratification in the Bay is weakest in October and November (Appendix 6), six months after peak Susquehanna River discharge in April (Schubel and Pritchard 1986). With increasing river discharge starting in the fall, stratification begins to increase during the winter and peaks in late spring and early summer. Starting in February as density stratification increases, strong vertical differences in surface versus subsurface temperature anomalies begin to appear until April and May where the majority of the channel exhibits these strong differences in temperature anomalies (Figure 3). In contrast, as density stratification becomes considerably weaker in the fall, the temperature anomalies become increasingly vertically homogenous (Figure 3).

There are, however, a few noteworthy exceptions to this general deep channel seasonal pattern, which are observed in shallow areas along the main stem, such as in the UB, LB, and the LC near the Rappahannock shoals. The UB is shallow (5-15m) with little to no stratification throughout the year, allowing temperature anomalies to penetrate to the bottom, except where fresh riverine waters and salty estuarine waters converge (Appendix 6). Since Susquehanna River

discharge controls circulation dynamics in the UB (Schubel and Pritchard 1986; Xiong et al. 2021), it is likely that variability in river discharge modulates the spatial distribution of this fresh and anomalously warm water mass.

In the LB, especially near the mouth of the CB, where tidal processes are strongest (Xiong et al. 2021), tidal mixing weakens the local vertical stratification (Guo and Valle-Levinson 2007), allowing for penetration of warmer waters below the average SML during fall-winter (Figure 3). However, during the summer, CB surface temperatures are much warmer than oceanic bottom waters entering the bay (Valle-Levinson 1995). This pattern is reflected in the slight thermal stratification of temperature anomalies during spring-summer MHW events (April to August) in the LB (Figure 3) and corresponds to elevated density stratification (Appendix 6). During the spring-summer, notable (1-2 °C) MHW anomalies do not penetrate the relatively cooler oceanic waters entering at the mouth of the CB, while in the fall-winter MHW anomalies were mixed throughout the water column. This highlights the importance of processes on daily or shorter time scales in the distribution of anomalous temperatures in the water column, and further research is required to address the impact of sub-daily processes on MHW dynamics.

Upstream of the Rappahannock Shoals in the deep channel (e.g., CBP station CB5.4; see Figure 1a), positive temperature anomalies were present during MHW events throughout the water column for most of the year (Figure 3). At the Rappahannock Shoals, vertical mixing is present year-round due to surface convergence and downwelling (Scully 2016b; Xiong et al. 2021) and is modulated by winds (Scully 2010a, 2016b). Brackish waters with elevated DO levels have been shown to be introduced to the LC by downwelling or mixing over the Rappahannock shoals (Scully 2016b), and are then transported upstream by gravitational circulation (Xiong et al. 2021). It is possible that heat is also transferred to the deep channel through this advective pathway during

spring-summer when stratification is enhanced, and in addition to lateral circulation, could explain small positive temperature anomalies (<1°C) observed below the SML during MHWs in the stratified season. A simple time-scale estimate using the average transport ($Q_E \sim 2400$ m^3 s^{-1}) across the deep channel calculated by Xiong et al. (2021) — ignoring efflux and reflux — and the volume below the pycnocline (V ~ 2.3 km^3; Scully 2016b) show that the timescale to fill the deep channel below the pycnocline is t ~ V/Q ~ 11 days, well within the timescale of stratified season preconditioning (i.e., pre-event priming of CB waters by elevated surface temperatures).

In addition to the seasonal variability in MLD, I have observed shoaling of the MLD (~2m) during MHW events (e.g., Figs. 2, 3, 6, 7). Yet this shoaling does not exceed one standard deviation of the $MLD_{\mu\ clim}$, which indicates that seasonal variability dominates the variability in stratification associated with anomalous warming during MHW events. This is largely due to seasonal stratification in the CB being dominated by salinity stratification due to river discharge, and not temperature stratification (Li et al. 2016). Stratification increases associated with anomalous temperatures during MHW events can be estimated using a linearized equation of state:

$$\Delta\rho_{Ta} = -\alpha\Delta T_a$$

where α, the thermal expansion coefficient, is equal to 0.25 kg m^{-3} °C^{-1}, and ΔT_a is the average surface-bottom difference in temperature anomalies. The proportion of $\Delta\rho_{Ta}$ (e.g., MHW temperature-induced changes to surface-bottom density) to the climatological surface-bottom density difference $\Delta\rho_{clim}$ indicates that MHW temperature changes account for only an ~5% increase in background stratification during the stratified season. This further supports the idea that seasonal stratification dominates the vertical structure of subsurface temperature anomalies during surface MHW events.

4.2 Dissolved Oxygen Spatiotemporal Variability

In contrast to the spatial structure in temperature anomalies during MHWs, which primarily varied with depth and were more horizontally homogeneous (Figure 3), DO anomalies varied widely both along the main stem and with depth in any given month (Figure 4). This highlights the more complex nature of DO dynamics, which are affected by a combination of physical and biogeochemical processes. I found that notable decreases (negative anomalies of 1-4 mg L^{-1}) in DO occurred below the MLD from late fall to early summer in the UB and channel during MHW events. In contrast, during the late summer and early fall, only small negative anomalies (less than 1 mg L-1) were present (Figure 4). However, these small DO anomalies coincided with the period of intense hypoxia and anoxia, which was already pervasive throughout much of the deep channel (Figure 4, Appendix 8). Thus, the MHW-associated decreases in DO, albeit small, still led to a sizable expansion of the hypoxic volume during this period. Furthermore, MHWs occurring in April and October could potentially be associated with an extended hypoxic season with an early initiation and delayed ending, respectively (Figure 4; Appendix 8). Additionally, surface blooms during MHWs (Appendix 7) could possibly provide a source of DO and cause supersaturation in the surface waters, negating DO reductions due to reduced solubility (Appendix 9).

It has been well documented that seasonal discharge, which inputs buoyancy and nutrients into the CB (enhancing stratification and eutrophication), controls bottom hypoxia and anoxia (Kemp et al. 2005; Li et al. 2016; Malone and Newton 2020). As shown by Scully (2013), elevated temperatures can also modulate the extent of low DO and hypoxia on synoptic timescales, which possibly occurred during the observed MHW events. From late fall to early summer, negative anomalies could partially (up to 30%) be attributed to a reduction in DO solubility due to warm

temperatures associated with MHWs in the UB and UC (Appendix 9). It is also possible that similar wind conditions that modulate hypoxia (i.e., down-estuary or up-estuary winds) (Wang 1979; Scully 2010a, 2016a) could also contribute to the onset or decline of MHWs in the Bay (Schaeffer and Roughan 2017; Holbrook et al. 2019; Ryan et al. 2021; Schlegel et al. 2021; Cook et al. 2022; Amaya et al. 2023a), causing a co-occurrence of low DO events and MHWs.

Yet, it is unlikely that low bottom DO is in response to enhanced subsurface respiration alone nor surface blooms during MHW events. The timescales for both oxygen drawdown and vertical fluxes of organic matter from blooms (and subsequent respiration; Appendix 7) are on the order of months (Appendix 8; Xiong and Shen 2022), though sinking rates do vary by phytoplankton community type (Spilling et al. 2018). Meanwhile, the average MHW in CB lasts ~11 days (Mazzini and Pianca 2022), a much shorter timescale. However, anomalous warming, and their effect on biogeochemical processes, was present for ~1-2 months preceding MHWs (Figure 6, 7). This is consistent with the timescale for oxygen drawdown and vertical fluxes, and therefore could potentially affect DO values that were observed during MHWs. Thus, low DO in the bottom waters is likely due to a combination of biogeochemical process prior to events and reduced solubility, enhanced respiration, and other physical processes (i.e., winds) during events.

Though disentangling the complex physical and biogeochemical mechanisms responsible for low DO and hypoxia/anoxia during MHW events is beyond the scope of this work, this analysis does demonstrate that reduced DO solubility due to elevated temperatures during MHWs is only responsible for a small fraction (up to ~30% change; Appendix 9) of the observed reduction in DO. Furthermore, the biogeochemical processes associated with the 1-2 months of anomalous warming preceding MHW events could potentially influence DO concentrations observed here and should be investigated in future work. Finally, as shown in this and other studies (Brauko et

al. 2020; Tassone et al. 2022; Lucey et al. 2022; Tomasetti et al. 2023), it is possible for low DO and MHWs to co-occur and compound each other. Future studies should address the mechanisms driving DO variability and how they interact with the extreme warming that occurs during MHW events in estuaries like the CB.

4.3 Marine Heatwave Drivers

Using a simple 1-D heat budget model, I found that air-estuary heat flux was the leading driver for the onsets (51.2%) and for a sizable portion of the declines (42.9%) of surface MHW events. These findings are largely consistent with Mazzini & Pianca (2021), who observed a large co-occurrence (50–65%) of MHW events between different regions of the CB and suggested that coherent large-scale air-sea heat fluxes were leading drivers of MHWs. Atmospheric forcing was also found to be the leading driver of the onset of surface MHWs across the broader Northwest Atlantic Continental Shelf (NWAS) (Chen et al. 2015; Schlegel et al. 2021; Perez et al. 2021; Großelindemann et al. 2022), but not during the declines (Schlegel et al. 2021). Though advection or vertical mixing, both of which were outside the scope of the methods in this study, likely played a more prominent role in MHW declines, atmospheric heat flux contributed substantially more to the decline of MHWs in this study in the CB ($\Delta T_{Qnet}/\Delta SSTa = 0.42$) than the NWAS ($\Delta T_{Qnet}/\Delta SSTa = -0.04$; Schlegel et al. 2021). As in the NWAS, I also found that latent heat flux was the leading constituent of the air-sea heat flux in the CB. A more detailed analysis of the atmospheric conditions and hydrodynamics preceding MHWs, as well as the triggering of MHWs is beyond the scope of the work, but should be pursued in future studies.

It is important to note that SML heat budget analysis for MHWs can be sensitive to the definition of the MLD (Elzahaby et al. 2022). During the spring and summer (stratified season),

the MLD and vertical penetration of temperature anomalies coincided, while during the fall and winter (homogeneous season), I identified a mismatch between these quantities, and therefore opted for a temperature anomaly definition of *H* in the simplified 1-D heat budget analysis (see eq. (3) and Section 2.5). It is possible that the mismatch was a result of sub-daily mixing by winds or tides, or the influence of synoptic weather systems, which are more frequent during fall and winter, but not captured in the CBP surveys. Cruise data are often collected during fair weather (CBP 2017), and thus stratification estimates are likely biased high. This highlights the necessity of continuous *in-situ* measurements distributed throughout the water column to fully understand the drivers and vertical distribution of MHWs.

Another factor important to the development of MHWs is preconditioning of the water column by drivers ranging from monthly to decadal timescales. This study showed that temperatures in the surface are on average anomalously warm for 1-2 months before MHW events, depending on the season (homogeneous versus stratified; Figure 6, 7). It is possible that large scale atmospheric conditions (i.e., high pressure system with atmospheric blocking), similarly observed in the NWAS (Chen et al. 2015; Perez et al. 2021), or anomalously fresh surface waters from elevated discharge or precipitation (Elzahaby and Schaeffer 2019; Scannell et al. 2020; Ryan et al. 2021), could prime estuarine waters and enhance MHWs in the Bay. Additionally, it is possible that basin-scale climate variability (e.g. North Atlantic Oscillation, Bermuda High Index and El Nino Southern Oscillation) , which increases the number of MHW days in the CB (Mazzini and Pianca 2022), could also precondition estuarine waters, as seen in other estuaries and the global oceans (Capotondi et al. 2022; Dalsin 2023). Further study is required to better understand large-scale weather patterns and conditions in the CB associated with MHW events.

4.4 Ecosystem Effects

The magnitude and duration of impacts associated with anomalous MHW warming ranges widely both geographically and across species (Suryan et al. 2021). In addition, the types of impacts an ecosystem or species experiences are also dependent on the season, as discussed by Großelindemann et al. (2022) in relation to the American lobster (*Homarus americanus*) in the NWAS. During summer MHWs, it is more likely that absolute temperatures will exceed organismal temperature tolerances, while during the winter season warmer temperatures are more likely to influence the life cycles of organisms (Großelindemann et al. 2022). An example in the CB is the blue crab (*Callinectes sapidus*), whose reproductive cycle and migration patterns are partially controlled by seasonal temperatures (Aguilar et al. 2005). It is possible that MHW temperature patterns could disrupt migration patterns by initiating them early or delaying them during the fall and winter when MHW temperature anomalies are greater and present throughout the water column (Figure 3), affecting fisheries. Additionally, the CB is a known fish nursery (Heck and Thoman 1984; Hartman and Brandt 1995; Jones 2014; Millette et al. 2020; Hyman et al. 2022), and MHWs have been shown to disrupt this ecosystem service, resulting in annual fin fishery declines (Colombano et al. 2022).

In the context of summertime thermal stress, Tassone et al. (2022) highlighted the importance of having a three-dimensional understanding of MHW structure to gauge whether there are thermal refuges present in an estuary or if migration is blocked. During the stratified season, the deep channel could possibly provide a thermal refuge during MHWs since subsurface temperature anomalies are minimal (Figure 3). However, during this season, the majority of the deep channel is hypoxic (Figure 4). This combination of anomalously warm temperatures in the

shallow waters and low DO in the deep channel could force a mass exodus of thermally intolerant mobile species from the CB. Future modeling studies need to address the three-dimensional spatial distribution of heat during MHW events across the entire Bay, including the shoals and tributaries, to better understand the potential total impact of MHW-induced stress on CB habitat.

Though the average MHW in the Bay lasts ~11 days (Mazzini and Pianca 2022), this study shows that temperatures can be elevated by several degrees for 4-20 days after events in the subsurface, depending on the season and location (Figure 6, 7). The persistence of elevated temperatures after MHWs has been found across the global oceans (Freeland and Ross 2019; Elzahaby and Schaeffer 2019; Scannell et al. 2020) and in other estuaries (Jackson et al. 2018). However, mesocosm experiments of MHW impacts on ecosystems are primarily designed to last the average length of MHW events in a given study region (Ehlers et al. 2008; Pansch et al. 2018; Seuront et al. 2019). Future experiments should consider the cumulative temperature stress or other thermal impacts due to warming that occurs over the course of weeks to months before and after individual MHW events in their experimental design. Additionally, these studies should assess the potential for multi-stressor systems and the compounding impacts of extreme temperatures coinciding with, for example, low DO.

As the Earth warms, MHWs have been increasing in frequency and intensity in the global oceans (Frölicher et al. 2018; Oliver 2019) and in estuaries (Mazzini and Pianca 2022; Cook et al. 2022). These trends are primarily driven by the long-term increase in mean temperature (Oliver 2019). The CB is warming faster in the summer (Hinson et al. 2021), indicating that the frequency and intensity of summer MHWs will likely increase more rapidly than winter MHWs. These greater intensities will exacerbate already declining DO levels due to reduced DO solubility (Irby et al. 2018). Additionally, increased stratification due to potentially increased precipitation

(St.Laurent et al. 2021) and river discharge, which may already reduce DO (Murphy et al. 2011; Ni et al. 2019), may amplify surface MHW intensity. This in turn could lead to further reductions in DO concentrations. Increased CB stratification due to sea level rise, increased precipitation, and river discharge could also lead to a reduction in the length of the homogenous MHW season. It is likely that the extreme temperatures during MHWs and low DO will increasingly compound habitat issues in the CB.

5. Conclusions

Due to the plethora of long-term and *in-situ* data in the CB, this study was able to characterize, for the first time: the spatial and temporal structure of subsurface temperature anomalies in the main stem associated with surface MHW events from daily to seasonal time scales; examine their impact on DO; and assess the role of air-sea heat flux as a driver in the onset and decline of MHWs in this large, temperate, partially mixed estuary common to many regions around the world.

Two distinct seasonal regimes of subsurface temperature anomalies were identified in association with surface MHWs in the CB: a thermally stratified spring-summer regime, when positive temperature anomalies were only present in the near-surface and were vertically capped by the MLD; and a thermally homogenous fall-winter regime, when positive anomalies were nearly constant throughout the water column. A simplified 1-D heat budget showed that air-sea heat fluxes were the leading drivers for most heatwaves in the CB; likewise, the seasonal vertical distribution of temperature anomalies were consistent with surface heating and seasonal changes in stratification in the Bay, controlled primarily by seasonal patterns in river discharge.

While temperature anomalies were horizontally and seasonally consistent across the CB, DO anomalies during MHWs varied widely, likely due to the more complex mechanisms that govern low DO in the CB. Negative DO anomalies were present throughout the main stem of the Bay, with the greatest DO decrease (~4 mg L^{-1}) during MHW events occurring in the UB and UC during the winter and spring. Notable DO decreases (>1 mg L^{-1}) occurred primarily in the winter and spring. While much smaller negative DO anomalies occurred during MHW events in the summer and fall, these anomalies occurred during times and in regions already experiencing critically low DO levels and led to an expansion of the hypoxic volume in the CB, as well as a potential increase in the hypoxic season.

This analysis also showed that positive surface temperature anomalies were present for approximately 1 month (homogeneous season) to 2 months (stratified season) before and after MHW events, and subsurface temperature anomalies were elevated for a few days to over a week before and up to two and a half weeks after events. This highlights that the timescales of elevated temperatures are typically much longer than the duration of individual MHW events and should be carefully considered in future laboratory and modeling studies attempting to assess thermal stress due to MHWs in the ecosystem.

While this work provides an initial analysis of the subsurface structure of temperature and DO anomalies associated with surface MHWs along the main stem of the CB, the cross-stem structure, the connection of such events with the CB tributaries and coastal plume (e.g., Mazzini et al. 2019), and the association of MHWs with changes in other biogeochemical parameters (e.g., chlorophyll, pH, turbidity) still need to be investigated. Future studies should also consider examining the role of local (e.g., winds, river discharge.) as well as regional drivers (e.g., North Atlantic Oscillation, Bermuda High Index, and El Nino Southern Oscillation), especially the role

of wet and dry years (an important source of variability in estuaries like CB) on estuarine MHW structure and dynamics, which I were unable to resolve with our dataset. Additionally, future studies should address the cumulative impact of MHWs on bottom DO and disentangle the complex mechanisms controlling DO dynamics in response to MHW events. In order to fully understand the structure, drivers, and dynamics of MHWs in these valuable ecosystems and assess MHW impacts in a changing climate, a systematic assessment of estuaries with varying types and morphologies, and use of higher spatial resolution data (both horizontally and vertically) from dedicated observational and modeling efforts are needed.

Appendix

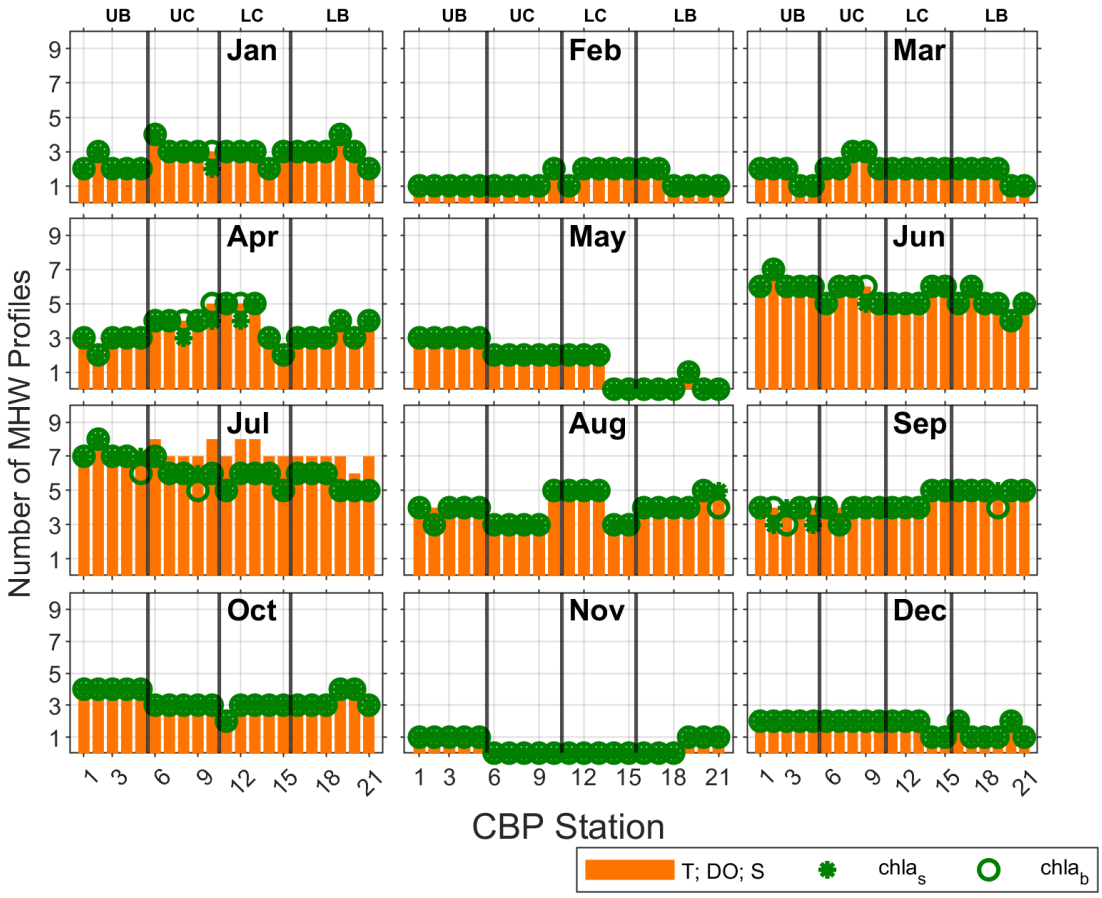

Appendix 1. Available Marine Heatwave (MHW) Profiles. MHW profiles per month per station for temperature, salinity, DO (orange bars), $CHLA_S$ (green asterisk), and $CHLA_B$ (green circle). Stations are numbered from the mouth of the Susquehanna River (1) to the mouth of the Chesapeake Bay (21). Vertical lines indicate the regions where the Chesapeake Bay stations are located. Abbreviations: Dissolved Oxygen (DO), Temperature (T), Salinity (S), Surface Chlorophyll ($CHLA_S$), Bottom Chlorophyll ($CHLA_B$), Upper Bay (UB), Upper Channel (UC), Lower Channel (LC), Lower Bay (LB).

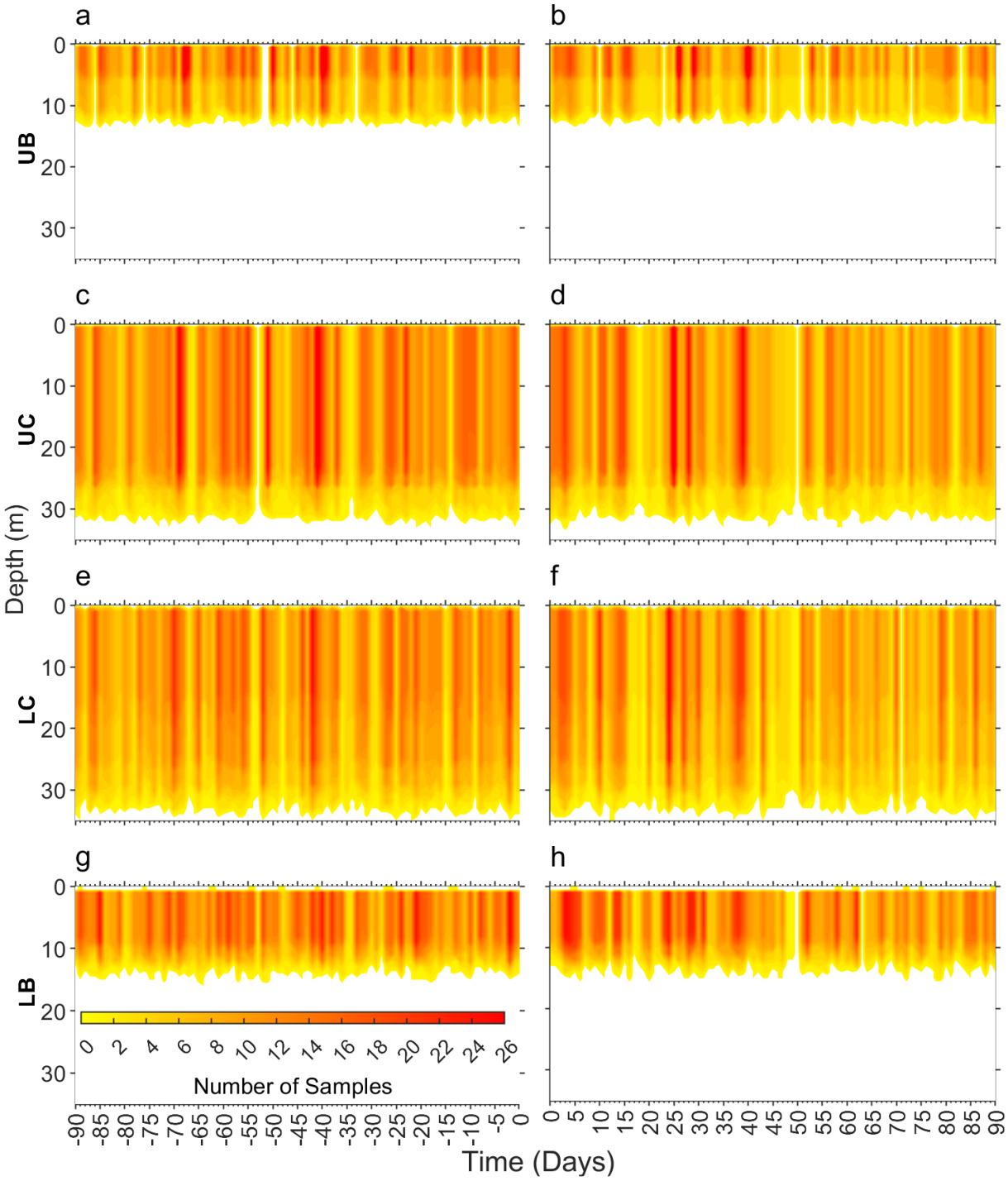

Appendix 2: Samples per Day Before and After Marine Heatwave (MHW) Events During the Stratified Season. Daily count of the number of samples collected during a surface marine heatwave at each depth and horizontal grid point during the stratified season (April to August; see Figure 6 or 7). White areas indicate no available data, and regions are indicated in the same way as Figure six.

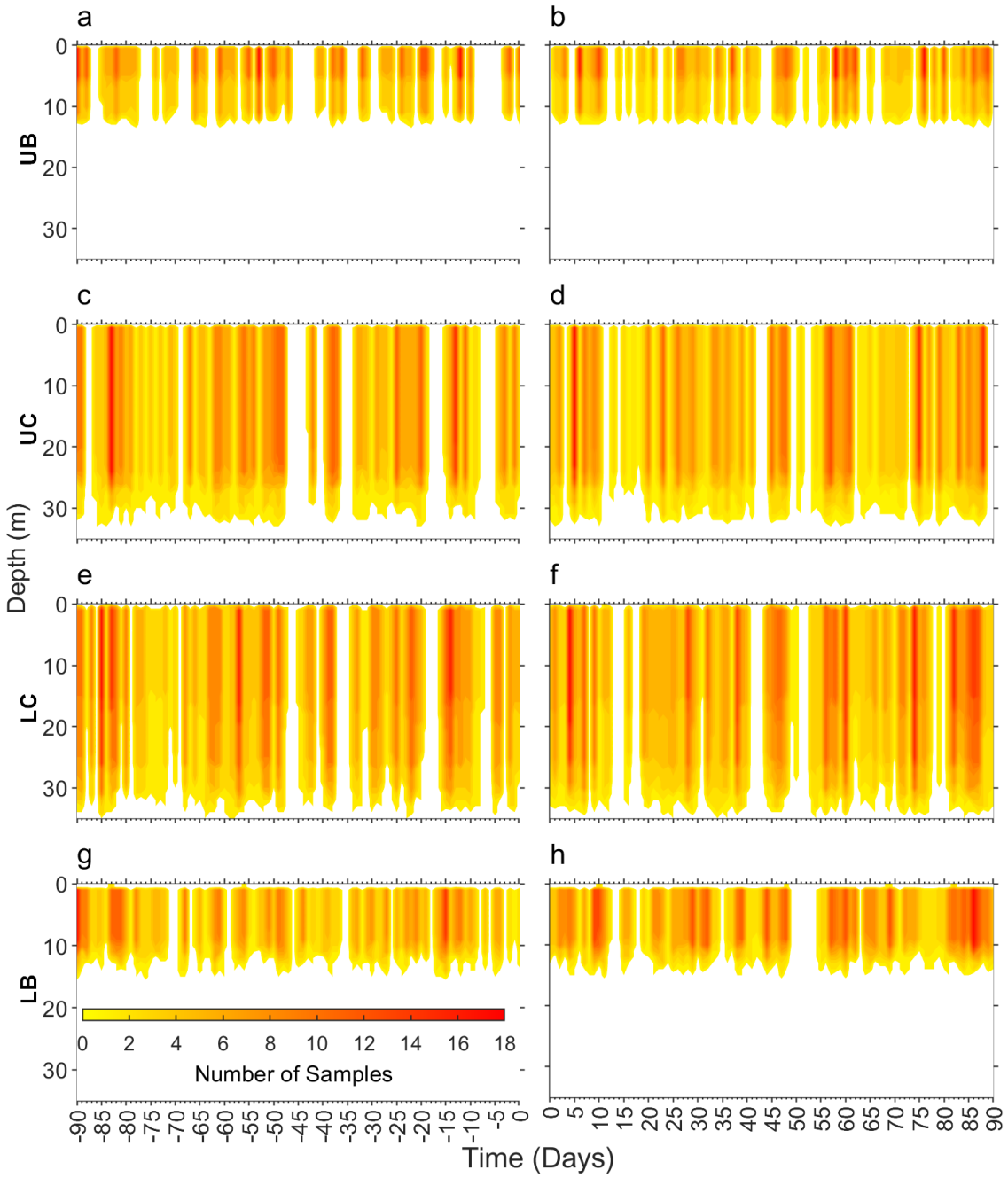

Appendix 3: Samples per Day Before and After Marine Heatwave (MHW) Events During the Homogenous Season. Daily count of the number of samples collected during a surface marine heatwave at each depth and horizontal grid point during the homogenous season (October to February; see Figure 6 or 7). White areas indicate no available data, and regions are indicated in the same way as in Figure 6.

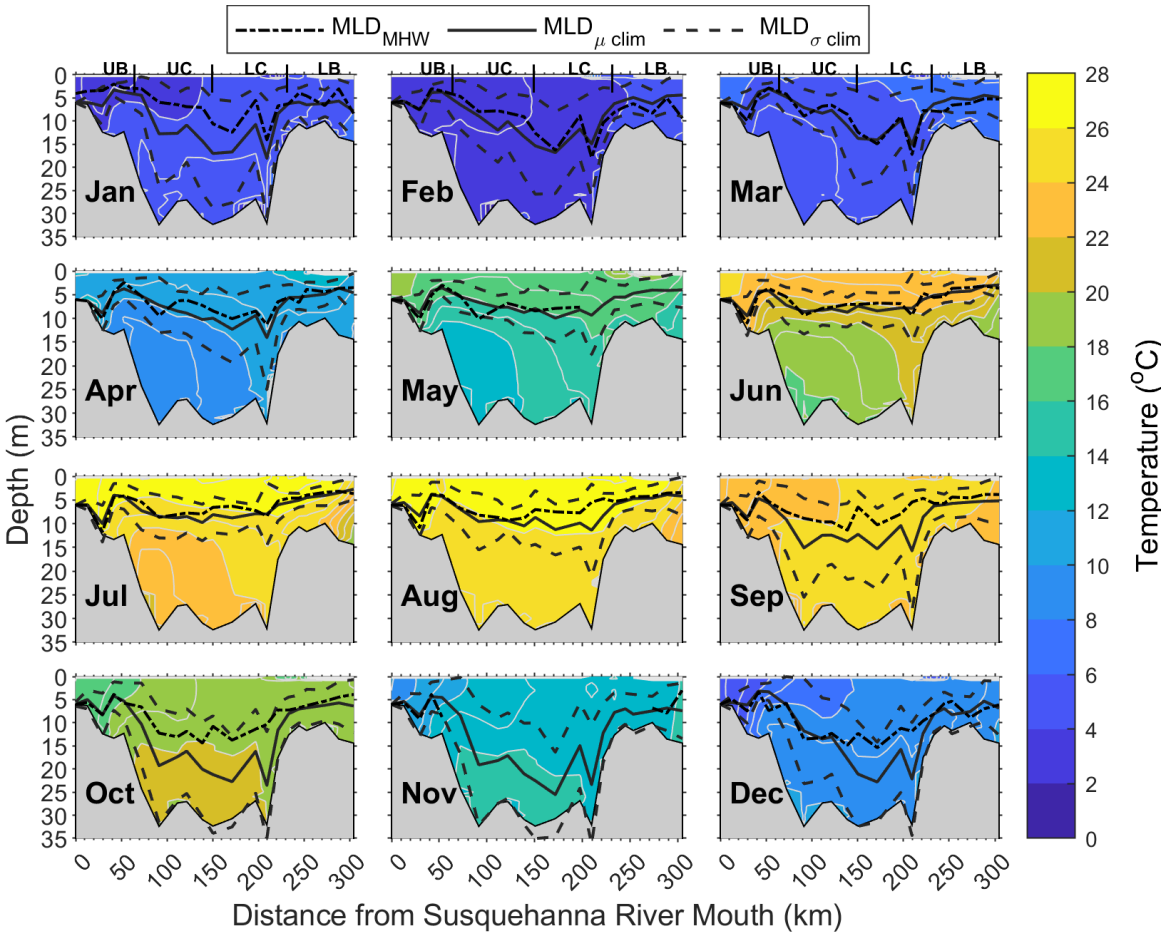

Appendix 4: Monthly Subsurface Temperature Climatology. Monthly average of temperature across the entire time series, with white contours indicating a change of 1 °C. For reference, the mean climatological mixed layer depth ($MLD_{\mu\ clim}$; solid grey line), standard deviation of the climatological mixed layer depth ($MLD_{\sigma\ clim}$; dashed grey line), and monthly averaged mixed layer depth during marine heatwave events (MLD_{MHW}; black dotted dashed line) are plotted. Regions are indicated in the same way as in Figure 3.

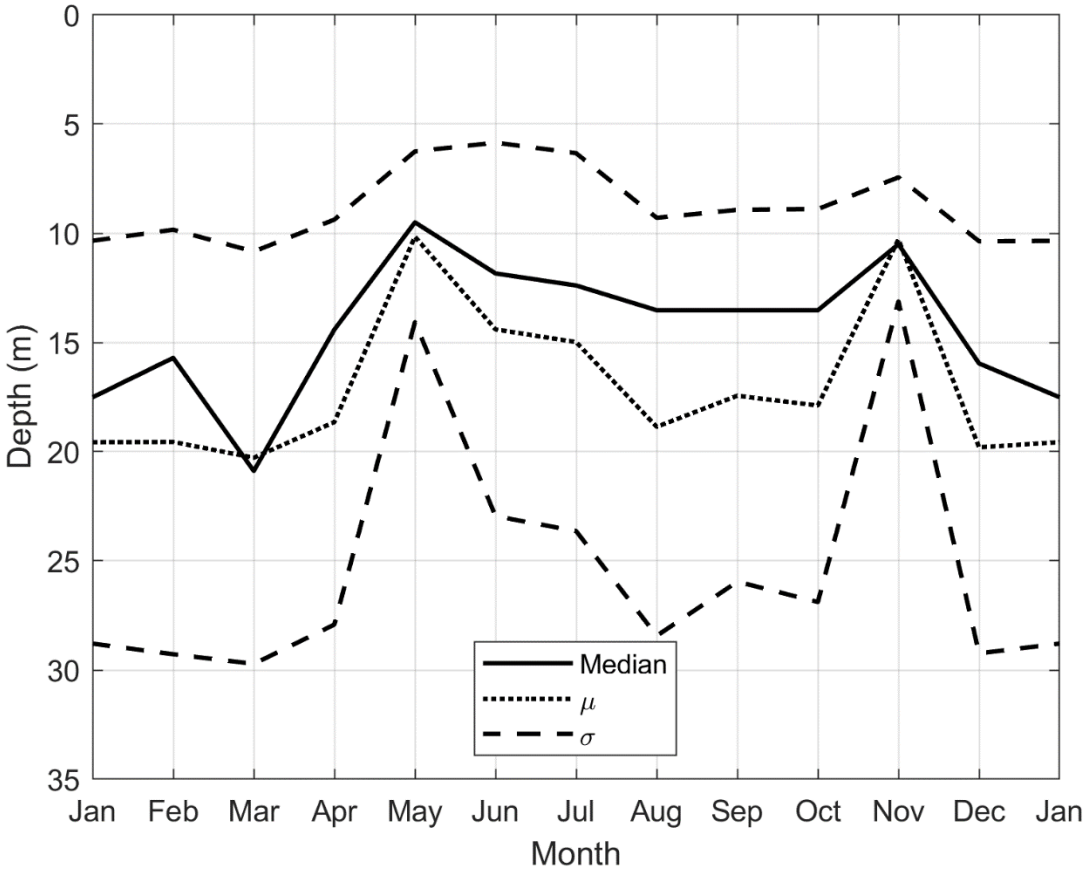

Appendix 5: Monthly Climatology of the Thermal Definition (H) of the Mixed Layer Depth. The monthly median (solid line), mean (dotted line), and standard deviation (dashed line) of the spatially averaged H.

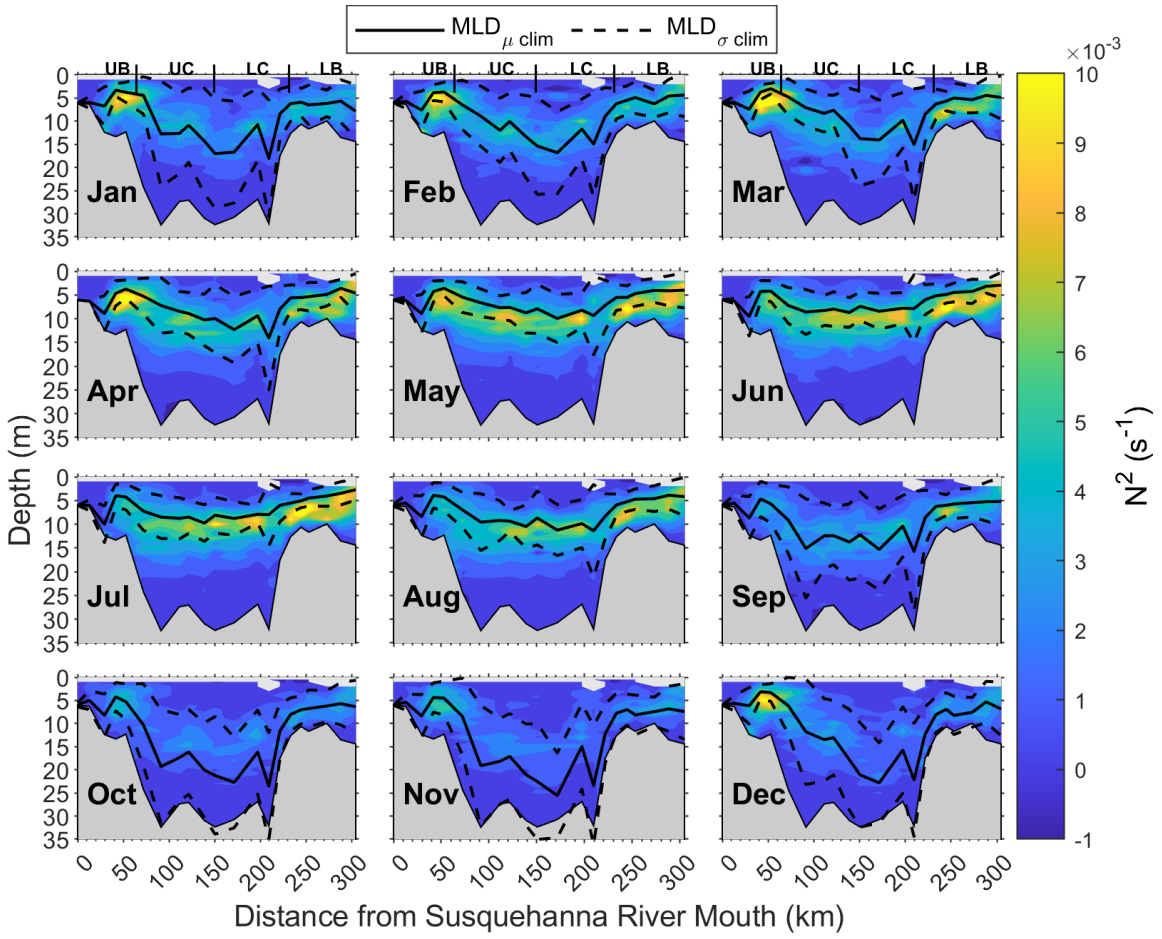

Appendix 6: Monthly Climatology of the Bouncy Frequency Squared (N^2) and Density Definition (MLD) of the Mixed Layer Depth. Monthly average of N^2 across the entire time series. For reference, the mean climatological mixed layer depth ($MLD_{\mu\ clim;}$ solid grey line), standard deviation of the climatological mixed layer depth ($MLD_{\sigma\ clim}$; dashed grey line) are plotted. Regions are indicated in the same way as in Figure 3.

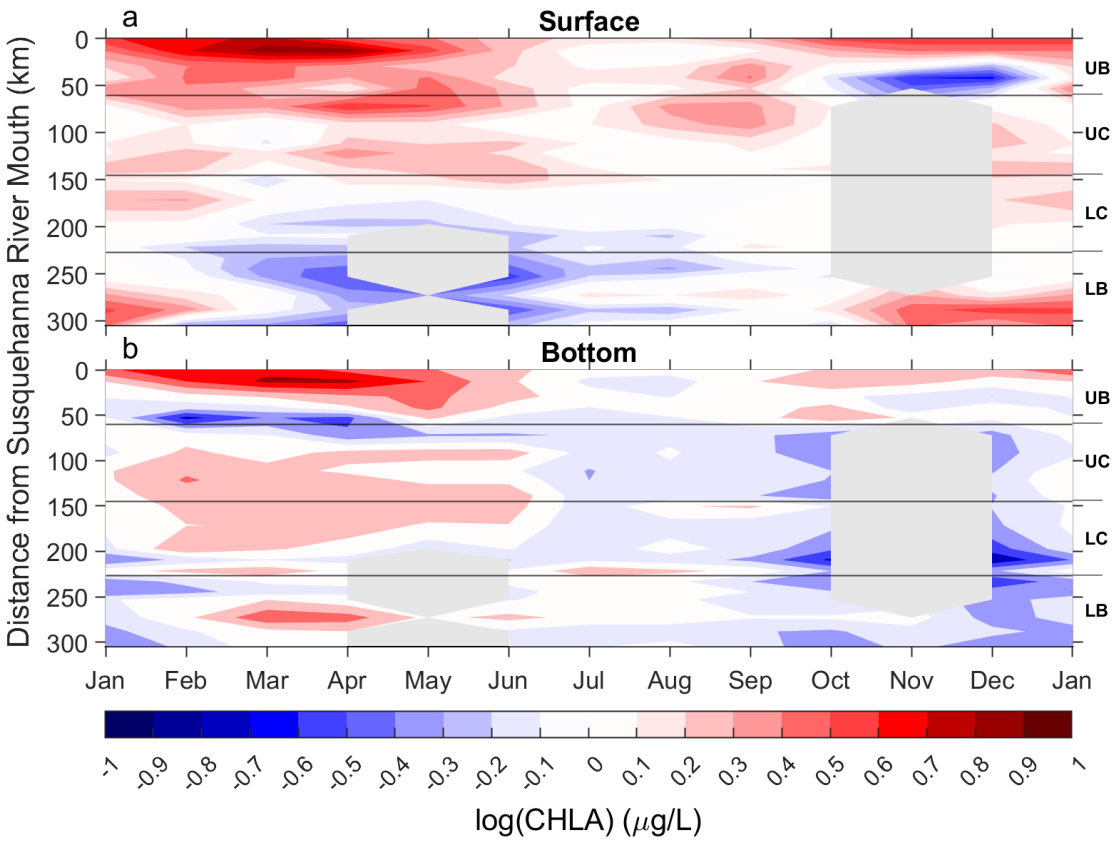

Appendix 7: Monthly Average Surface and Bottom Chlorophyll Anomalies During Surface Marine Heatwave (MHW) Events. Monthly mean Surface (a) and Bottom (b) chlorophyll anomalies. The grey horizontal lines indicate the regions of the Bay, Upper Bay (UB), Upper Channel (UC), Lower Channel (LC), Lower Bay (LB) and the grey shaded indicate missing data. A three-month moving average was applied during months with low data availability (see Appendix 1).

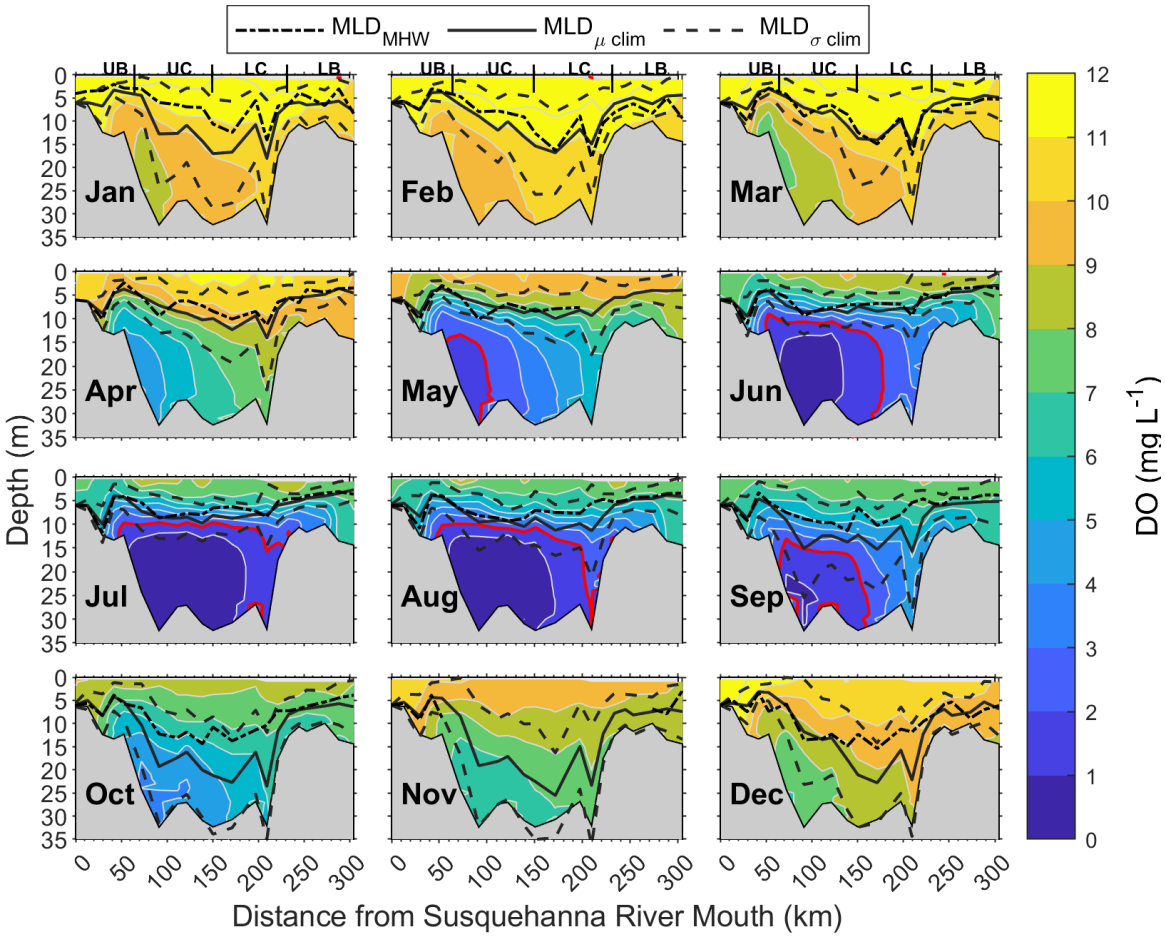

Appendix 8: Monthly Climatology of Subsurface Dissolved Oxygen (DO). Monthly average of DO across the entire time series, with white contours indicating a change of 1 mg L^{-1} and the red contour indicating hypoxia (DO < 2 mg L^{-1}). For reference, the mean climatological mixed layer depth ($MLD_{\mu\ clim}$; solid grey line), standard deviation of the climatological mixed layer depth ($MLD_{\sigma\ clim}$; dashed grey line), and monthly averaged mixed layer depth during marine heatwave events (MLD_{MHW}; black dotted dashed line) are plotted. Regions are indicated in the same way as in Figure 3.

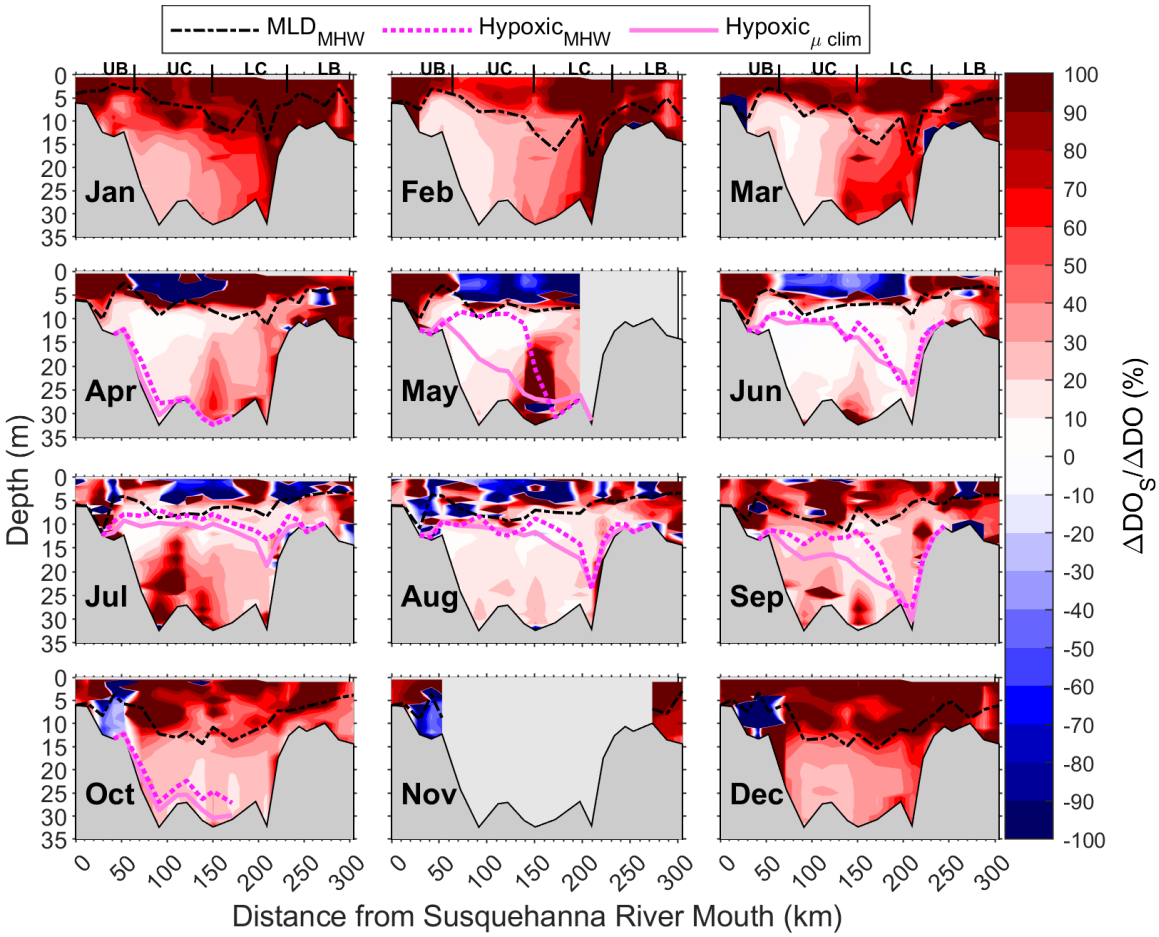

Appendix 9: Monthly Average Proportion of Dissolved Oxygen (DO) Change due to the Change in DO Solubility. Each point is the monthly average of the proportions of DO change due to the change in DO solubility. The average monthly marine heatwave mixed layer depth (MLD_{MHW}), hypoxic contour ($Hypoxic_{MHW}$) and climatological hypoxic contour ($Hypoxic_{\mu\ clim}$) are indicated in the same way as Figure 4 in addition to regions of the Bay.

Literature Cited

Aguilar R, Hines AH, Wolcott TG, et al (2005) The timing and route of movement and migration of post-copulatory female blue crabs, Callinectes sapidus Rathbun, from the upper Chesapeake Bay. Journal of Experimental Marine Biology and Ecology 319:117–128. https://doi.org/10.1016/j.jembe.2004.08.030

Alosairi Y, Alsulaiman N, Rashed A, Al-Houti D (2020) World record extreme sea surface temperatures in the northwestern Arabian/Persian Gulf verified by in situ measurements. Marine Pollution Bulletin 161:111766. https://doi.org/10.1016/j.marpolbul.2020.111766

Amaya DJ, Jacox MG, Alexander MA, et al (2023a) Bottom marine heatwaves along the continental shelves of North America. Nat Commun 14:1038. https://doi.org/10.1038/s41467-023-36567-0

Amaya DJ, Jacox MG, Fewings MR, et al (2023b) Marine heatwaves need clear definitions so coastal communities can adapt. Nature 616:29–32. https://doi.org/10.1038/d41586-023-00924-2

Anderson GF (2021) Vims Ferry Pier Ambient Water Monitoring, Salinity and Temperature, Daily Summary 1947-2003. William & Mary

Aoki LR, McGlathery KJ, Wiberg PL, et al (2021) Seagrass Recovery Following Marine Heat Wave Influences Sediment Carbon Stocks. Front Mar Sci 7:576784. https://doi.org/10.3389/fmars.2020.576784

Ashizawa D, Cole JJ (1994) Long-Term Temperature Trends of the Hudson River: A Study of the Historical Data. Estuaries 17:166. https://doi.org/10.2307/1352565

Bass AV, Smith KE, Smale DA (2023) Marine heatwaves and decreased light availability interact to erode the ecophysiological performance of habitat-forming kelp species. Journal of Phycology jpy.13332. https://doi.org/10.1111/jpy.13332

Brauko KM, Cabral A, Costa NV, et al (2020) Marine Heatwaves, Sewage and Eutrophication Combine to Trigger Deoxygenation and Biodiversity Loss: A SW Atlantic Case Study. Front Mar Sci 7:590258. https://doi.org/10.3389/fmars.2020.590258

Cai X, Shen J, Zhang YJ, et al (2021) Impacts of Sea-Level Rise on Hypoxia and Phytoplankton Production in Chesapeake Bay: Model Prediction and Assessment. J Am Water Resour Assoc 1752–1688.12921. https://doi.org/10.1111/1752-1688.12921

Capotondi A, Newman M, Xu T, Di Lorenzo E (2022) An Optimal Precursor of Northeast Pacific Marine Heatwaves and Central Pacific El Niño Events. Geophysical Research Letters 49:. https://doi.org/10.1029/2021GL097350

Caputi N, Kangas M, Denham A, et al (2016) Management adaptation of invertebrate fisheries to an extreme marine heat wave event at a global warming hot spot. Ecol Evol 6:3583–3593. https://doi.org/10.1002/ece3.2137

CBP (2017) Methods and Qulity Assurance for Chesapeake Bay Water Quality Monitoring Programs

Chen K, Gawarkiewicz G, Kwon Y, Zhang WG (2015) The role of atmospheric forcing versus ocean advection during the extreme warming of the Northeast U.S. continental shelf in 2012. J Geophys Res Oceans 120:4324–4339. https://doi.org/10.1002/2014JC010547

Cheung WWL, Frölicher TL (2020) Marine heatwaves exacerbate climate change impacts for fisheries in the northeast Pacific. Sci Rep 10:6678. https://doi.org/10.1038/s41598-020-63650-z

Cloern JE, Foster SQ, Kleckner AE (2014) Phytoplankton primary production in the world's estuarine-coastal ecosystems. Biogeosciences 11:2477–2501. https://doi.org/10.5194/bg-11-2477-2014

Colombano DD, Carlson SM, Hobbs JA, Ruhi A (2022) Four decades of climatic fluctuations and fish recruitment stability across a marine-freshwater gradient. Global Change Biology 28:5104–5120. https://doi.org/10.1111/gcb.16266

Cook F, Smith RO, Roughan M, et al (2022) Marine heatwaves in shallow coastal ecosystems are coupled with the atmosphere: Insights from half a century of daily in situ temperature records. Front Clim 4:1012022. https://doi.org/10.3389/fclim.2022.1012022

Cronin TM, Dwyer GS, Kamiya T, et al (2003) Medieval Warm Period, Little Ice Age and 20th century temperature variability from Chesapeake Bay. Global and Planetary Change 36:17–29. https://doi.org/10.1016/S0921-8181(02)00161-3

Dalsin M (2023) Effects of basin-scale climate modes and upwelling on nearshore marine heatwaves and cold spells in the California Current. Scientific Reports

Du J, Shen J (2015) Decoupling the influence of biological and physical processes on the dissolved oxygen in the Chesapeake Bay. J Geophys Res Oceans 120:78–93. https://doi.org/10.1002/2014JC010422

Du J, Shen J (2016) Water residence time in Chesapeake Bay for 1980–2012. Journal of Marine Systems 164:101–111. https://doi.org/10.1016/j.jmarsys.2016.08.011

Eakin CM, Sweatman HPA, Brainard RE (2019) The 2014–2017 global-scale coral bleaching event: insights and impacts. Coral Reefs 38:539–545. https://doi.org/10.1007/s00338-019-01844-2

Ehlers A, Worm B, Reusch T (2008) Importance of genetic diversity in eelgrass Zostera marina for its resilience to global warming. Mar Ecol Prog Ser 355:1–7. https://doi.org/10.3354/meps07369

Elzahaby Y, Schaeffer A (2019) Observational Insight Into the Subsurface Anomalies of Marine Heatwaves. Front Mar Sci 6:745. https://doi.org/10.3389/fmars.2019.00745

Elzahaby Y, Schaeffer A, Roughan M, Delaux S (2022) Why the Mixed Layer Depth Matters When Diagnosing Marine Heatwave Drivers Using a Heat Budget Approach. Front Clim 4:838017. https://doi.org/10.3389/fclim.2022.838017

Filbee-Dexter K, Wernberg T, Grace SP, et al (2020) Marine heatwaves and the collapse of marginal North Atlantic kelp forests. Sci Rep 10:13388. https://doi.org/10.1038/s41598-020-70273-x

Frankel LT, Friedrichs MAM, St-Laurent P, et al (2022) Nitrogen reductions have decreased hypoxia in the Chesapeake Bay: Evidence from empirical and numerical modeling. Science of The Total Environment 814:152722. https://doi.org/10.1016/j.scitotenv.2021.152722

Freeland H, Ross T (2019) 'The Blob' - or, how unusual were ocean temperatures in the Northeast Pacific during 2014-2018? Deep Sea Research Part I: Oceanographic Research Papers 150:103061. https://doi.org/10.1016/j.dsr.2019.06.007

Frölicher TL, Fischer EM, Gruber N (2018) Marine heatwaves under global warming. Nature 560:360–364. https://doi.org/10.1038/s41586-018-0383-9

Garvine RW (1985) A Simple Model of Estuarine Subtidal Fluctuations Forced by Local and Remote Wind Stress. Journal of Geophysical Research 90:11945–11948

Großelindemann H, Ryan S, Ummenhofer CC, et al (2022) Marine Heatwaves and Their Depth Structures on the Northeast U.S. Continental Shelf. Front Clim 4:857937. https://doi.org/10.3389/fclim.2022.857937

Guo X, Valle-Levinson A (2007) Tidal effects on estuarine circulation and outflow plume in the Chesapeake Bay. Continental Shelf Research 27:20–42. https://doi.org/10.1016/j.csr.2006.08.009

Hartman KJ, Brandt SB (1995) Predatory deman and impact of striped bass, bluefish, and weakfish in the Chesapeake Bay: applications of bioenergetics models. Canadian Journal of Fisheries and Aquatic Sciences 52:1667–1687

Heck KL, Thoman TA (1984) The Nursery Role of Seagrass Meadows in the Upper and Lower Reaches of the Chesapeake Bay. Estuaries 7:70. https://doi.org/10.2307/1351958

Hersbach H, Bell B, Berrisford P, et al (2018) ERA5 hourly data on pressure levels from 1959 to present. Copernicus Climate Change Service (C3S) Climate Data Store (CDS)

Hinson KE, Friedrichs MAM, Najjar RG, et al (2023) Impacts and uncertainties of climate-induced changes in watershed inputs on estuarine hypoxia. Biogeosciences 20:1937–1961. https://doi.org/10.5194/bg-20-1937-2023

Hinson KE, Friedrichs MAM, St-Laurent P, et al (2021) Extent and Causes of Chesapeake Bay Warming. J Am Water Resour Assoc 1752–1688.12916. https://doi.org/10.1111/1752-1688.12916

Holbrook NJ, Scannell HA, Sen Gupta A, et al (2019) A global assessment of marine heatwaves and their drivers. Nat Commun 10:2624. https://doi.org/10.1038/s41467-019-10206-z

Holser RR, Keates TR, Costa DP, Edwards CA (2022) Extent and Magnitude of Subsurface Anomalies During the Northeast Pacific Blob as Measured by Animal-Borne Sensors. JGR Oceans 127:. https://doi.org/10.1029/2021JC018356

Hu S, Li S, Zhang Y, et al (2021) Observed strong subsurface marine heatwaves in the tropical western Pacific Ocean. Environ Res Lett 16:104024. https://doi.org/10.1088/1748-9326/ac26f2

Hughes TP, Kerry JT, Álvarez-Noriega M, et al (2017) Global warming and recurrent mass bleaching of corals. Nature 543:373–377. https://doi.org/10.1038/nature21707

Hyman AC, Chiu GS, Fabrizio MC, Lipcius RN (2022) Spatiotemporal Modeling of Nursery Habitat Using Bayesian Inference: Environmental Drivers of Juvenile Blue Crab Abundance. Front Mar Sci 9:834990. https://doi.org/10.3389/fmars.2022.834990

Irby ID, Friedrichs MAM, Da F, Hinson KE (2018) The competing impacts of climate change and nutrient reductions on dissolved oxygen in Chesapeake Bay. Biogeosciences 15:2649–2668. https://doi.org/10.5194/bg-15-2649-2018

Jackson JM, Johnson GC, Dosser HV, Ross T (2018) Warming From Recent Marine Heatwave Lingers in Deep British Columbia Fjord. Geophys Res Lett 45:9757–9764. https://doi.org/10.1029/2018GL078971

Jacox MG (2019) Marine heatwaves in a changing climate. Nature 571:485–487. https://doi.org/10.1038/d41586-019-02196-1

Jones CM (2014) Can we predict the future: juvenile finfish and their seagrass nurseries in the Chesapeake Bay. ICES Journal of Marine Science 71:681–688. https://doi.org/10.1093/icesjms/fst142

JPL-MUR-MeaSUREs-Project (2015) Ghrsst Level 4 Mur Global Foundation Sea Surface Temperature Analysis (v4.1). PO.DAAC,CA

Kemp W, Boynton W, Adolf J, et al (2005) Eutrophication of Chesapeake Bay: historical trends and ecological interactions. Mar Ecol Prog Ser 303:1–29. https://doi.org/10.3354/meps303001

Lee M-A, Tzeng M-T, Hosoda K, et al (2010) Validation of JAXA/MODIS Sea Surface Temperature in Water around Taiwan Using the Terra and Aqua Satellites. Terr Atmos Ocean Sci 21:727–736. https://doi.org/doi: 10.3319/TAO.2009.09.07.01

Lee YJ, Boynton WR, Li M, Li Y (2013) Role of Late Winter–Spring Wind Influencing Summer Hypoxia in Chesapeake Bay. Estuaries and Coasts 36:683–696. https://doi.org/10.1007/s12237-013-9592-5

Li M, Lee YJ, Testa JM, et al (2016) What drives interannual variability of hypoxia in Chesapeake Bay: Climate forcing versus nutrient loading? Geophys Res Lett 43:2127–2134. https://doi.org/10.1002/2015GL067334

Li Y, Li M (2011) Effects of winds on stratification and circulation in a partially mixed estuary. J Geophys Res 116:C12012. https://doi.org/10.1029/2010JC006893

Lonhart SI, Jeppesen R, Beas-Luna R, et al (2019) Shifts in the distribution and abundance of coastal marine species along the eastern Pacific Ocean during marine heatwaves from 2013 to 2018. Mar Biodivers Rec 12:13. https://doi.org/10.1186/s41200-019-0171-8

Lucey N, Aube C, Herwig A, Collin R (2022) Compound Extreme Events Induce Rapid Mortality in a Tropical Sea Urchin. The Biological Bulletin 243:239–254. https://doi.org/10.1086/722283

Magel CL, Chan F, Hessing-Lewis M, Hacker SD (2022) Differential Responses of Eelgrass and Macroalgae in Pacific Northwest Estuaries Following an Unprecedented NE Pacific Ocean Marine Heatwave. Front Mar Sci 9:838967. https://doi.org/10.3389/fmars.2022.838967

Malone TC, Newton A (2020) The Globalization of Cultural Eutrophication in the Coastal Ocean: Causes and Consequences. Front Mar Sci 7:670. https://doi.org/10.3389/fmars.2020.00670

Marin Jarrin MJ, Sutherland DA, Helms AR (2022) Water temperature variability in the Coos Estuary and its potential link to eelgrass loss. Front Mar Sci 9:930440. https://doi.org/10.3389/fmars.2022.930440

Marin M, Feng M, Phillips HE, Bindoff NL (2021) A Global, Multiproduct Analysis of Coastal Marine Heatwaves: Distribution, Characteristics, and Long-Term Trends. J Geophys Res Oceans 126:. https://doi.org/10.1029/2020JC016708

Mazzini PLF, Chant RJ, Scully ME, et al (2019) The Impact of Wind Forcing on the Thermal Wind Shear of A River Plume. J Geophys Res Oceans 124:7908–7925. https://doi.org/10.1029/2019JC015259

Mazzini PLF, Pianca C (2022) Marine Heatwaves in the Chesapeake Bay. Front Mar Sci 8:750265. https://doi.org/10.3389/fmars.2021.750265

McCabe RM, Hickey BM, Kudela RM, et al (2016) An unprecedented coastwide toxic algal bloom linked to anomalous ocean conditions. Geophys Res Lett 43:. https://doi.org/10.1002/2016GL070023

McDougall TJ, Barker PM (2011) Getting started with TEOS-10 and the Gibbs Seawater (GSW) Oceanographic Toolbox,. SCOR/IAPSO WG127

Millette NC, Pierson JJ, North EW (2020) Water temperature during winter may control striped bass recruitment during spring by affecting the development time of copepod nauplii. ICES Journal of Marine Science 77:300–314. https://doi.org/10.1093/icesjms/fsz203

Moisan JR, Niiler PP (1998) The Seasonal Heat Budget of the North Pacific: Net Heat Flux and Heat Storage Rates (1950–1990). J Phys Oceanogr 28:401–421. https://doi.org/10.1175/1520-0485(1998)028<0401:TSHBOT>2.0.CO;2

Murphy RR, Keisman J, Harcum J, et al (2022) Nutrient Improvements in Chesapeake Bay: Direct Effect of Load Reductions and Implications for Coastal Management. Environ Sci Technol 56:260–270. https://doi.org/10.1021/acs.est.1c05388

Murphy RR, Kemp WM, Ball WP (2011) Long-Term Trends in Chesapeake Bay Seasonal Hypoxia, Stratification, and Nutrient Loading. Estuaries and Coasts 34:1293–1309. https://doi.org/10.1007/s12237-011-9413-7

Najjar RG, Pyke CR, Adams MB, et al (2010) Potential climate-change impacts on the Chesapeake Bay. Estuarine, Coastal and Shelf Science 86:1–20. https://doi.org/10.1016/j.ecss.2009.09.026

Ni W, Li M, Ross AC, Najjar RG (2019) Large Projected Decline in Dissolved Oxygen in a Eutrophic Estuary Due to Climate Change. J Geophys Res Oceans 124:8271–8289. https://doi.org/10.1029/2019JC015274

Oczkowski A, McKinney R, Ayvazian S, et al (2015) Preliminary Evidence for the Amplification of Global Warming in Shallow, Intertidal Estuarine Waters. PLoS ONE 10:e0141529. https://doi.org/10.1371/journal.pone.0141529

Oliver ECJ (2019) Mean warming not variability drives marine heatwave trends. Clim Dyn 53:1653–1659. https://doi.org/10.1007/s00382-019-04707-2

Oliver ECJ, Benthuysen JA, Darmaraki S, et al (2021) Marine Heatwaves. Annu Rev Mar Sci 13:313–342. https://doi.org/10.1146/annurev-marine-032720-095144

Oliver ECJ, Burrows MT, Donat MG, et al (2019) Projected Marine Heatwaves in the 21st Century and the Potential for Ecological Impact. Front Mar Sci 6:734. https://doi.org/10.3389/fmars.2019.00734

Oliver ECJ, Lago V, Hobday AJ, et al (2018) Marine heatwaves off eastern Tasmania: Trends, interannual variability, and predictability. Progress in Oceanography 161:116–130. https://doi.org/10.1016/j.pocean.2018.02.007

Pansch C, Scotti M, Barboza FR, et al (2018) Heat waves and their significance for a temperate benthic community: A near-natural experimental approach. Glob Change Biol 24:4357–4367. https://doi.org/10.1111/gcb.14282

Perez E, Ryan S, Andres M, et al (2021) Understanding physical drivers of the 2015/16 marine heatwaves in the Northwest Atlantic. Sci Rep 11:17623. https://doi.org/10.1038/s41598-021-97012-0

Preston BL (2004) Observed Winter Warming of the Chesapeake Bay Estuary (1949?2002): Implications for Ecosystem Management. Environmental Management 34:. https://doi.org/10.1007/s00267-004-0159-x

Rice KC, Jastram JD (2015) Rising air and stream-water temperatures in Chesapeake Bay region, USA. Climatic Change 128:127–138. https://doi.org/10.1007/s10584-014-1295-9

Ross AC, Stock CA (2022) Probabilistic extreme SST and marine heatwave forecasts in Chesapeake Bay: A forecast model, skill assessment, and potential value. Front Mar Sci 9:896961. https://doi.org/10.3389/fmars.2022.896961

Ryan S, Ummenhofer CC, Gawarkiewicz G, et al (2021) Depth Structure of Ningaloo Niño/Niña Events and Associated Drivers. Journal of Climate 34:1767–1788. https://doi.org/10.1175/JCLI-D-19-1020.1

Sanford E, Sones JL, García-Reyes M, et al (2019) Widespread shifts in the coastal biota of northern California during the 2014–2016 marine heatwaves. Sci Rep 9:4216. https://doi.org/10.1038/s41598-019-40784-3

Scannell HA, Johnson GC, Thompson L, et al (2020) Subsurface Evolution and Persistence of Marine Heatwaves in the Northeast Pacific. Geophys Res Lett 47:. https://doi.org/10.1029/2020GL090548

Schaeffer A, Roughan M (2017) Subsurface intensification of marine heatwaves off southeastern Australia: The role of stratification and local winds: SUBSURFACE MARINE HEAT WAVES. Geophys Res Lett 44:5025–5033. https://doi.org/10.1002/2017GL073714

Schlegel RW, Oliver ECJ, Chen K (2021) Drivers of Marine Heatwaves in the Northwest Atlantic: The Role of Air–Sea Interaction During Onset and Decline. Front Mar Sci 8:627970. https://doi.org/10.3389/fmars.2021.627970

Schlegel RW, Oliver ECJ, Hobday AJ, Smit AJ (2019) Detecting Marine Heatwaves With Sub-Optimal Data. Front Mar Sci 6:737. https://doi.org/10.3389/fmars.2019.00737

Schubel JR, Pritchard DW (1986) Responses of Upper Chesapeake Bay to Variations in Discharge of the Susquehanna River. Estuaries 9:236–239

Scully ME (2010a) Wind Modulation of Dissolved Oxygen in Chesapeake Bay. Estuaries and Coasts 33:1164–1175. https://doi.org/10.1007/s12237-010-9319-9

Scully ME (2010b) The Importance of Climate Variability to Wind-Driven Modulation of Hypoxia in Chesapeake Bay. Journal of Physical Oceanography 40:1435–1440. https://doi.org/10.1175/2010JPO4321.1

Scully ME (2016a) The contribution of physical processes to inter-annual variations of hypoxia in Chesapeake Bay: A 30-yr modeling study. Limnol Oceanogr 61:2243–2260. https://doi.org/10.1002/lno.10372

Scully ME (2016b) Mixing of dissolved oxygen in Chesapeake Bay driven by the interaction between wind-driven circulation and estuarine bathymetry. Journal of Geophysical Research: Oceans 121:5639–5654. https://doi.org/10.1002/2016JC011924

Seekell DA, Pace ML (2011) Climate change drives warming in the hudson river estuary, new york (usa). J Environ Monit 13:2321–2327

Seuront L, Nicastro KR, Zardi GI, Goberville E (2019) Decreased thermal tolerance under recurrent heat stress conditions explains summer mass mortality of the blue mussel Mytilus edulis. Sci Rep 9:17498. https://doi.org/10.1038/s41598-019-53580-w

Shields E, Moore K, Parrish D (2018) Adaptations by Zostera marina Dominated Seagrass Meadows in Response to Water Quality and Climate Forcing. Diversity 10:125. https://doi.org/10.3390/d10040125

Snyder JT, Whitney MM, Dam HG, et al (2019) Citizen science observations reveal rapid, multi-decadal ecosystem changes in eastern Long Island Sound. Marine Environmental Research 146:80–88. https://doi.org/10.1016/j.marenvres.2019.03.007

Spilling K, Olli K, Lehtoranta J, et al (2018) Shifting Diatom—Dinoflagellate Dominance During Spring Bloom in the Baltic Sea and its Potential Effects on Biogeochemical Cycling. Front Mar Sci 5:327. https://doi.org/10.3389/fmars.2018.00327

St.Laurent KA, Coles VJ, Hood RR (2021) Climate Extremes and Variability Surrounding Chesapeake Bay: Past, Present, and Future. J American Water Resour Assoc 1752–1688.12945. https://doi.org/10.1111/1752-1688.12945

Strydom S, Murray K, Wilson S, et al (2020) Too hot to handle: Unprecedented seagrass death driven by marine heatwave in a World Heritage Area. Glob Change Biol 26:3525–3538. https://doi.org/10.1111/gcb.15065

Suryan RM, Arimitsu ML, Coletti HA, et al (2021) Ecosystem response persists after a prolonged marine heatwave. Sci Rep 11:6235. https://doi.org/10.1038/s41598-021-83818-5

Tassone SJ, Besterman AF, Buelo CD, et al (2022) Co-occurrence of Aquatic Heatwaves with Atmospheric Heatwaves, Low Dissolved Oxygen, and Low pH Events in Estuarine Ecosystems. Estuaries and Coasts 45:707–720. https://doi.org/10.1007/s12237-021-01009-x

Thomson RE, Emery WJ (2014) Chapter 3 - Statistical Methods and Error Handling. In: Data Analysis Methods in Physical Oceanography, 3rd edn. Elsevier, pp 219–311

Tomasetti SJ, Hallinan BD, Tettelbach ST, et al (2023) Warming and hypoxia reduce the performance and survival of northern bay scallops (*Argopecten irradians irradians*) amid a fishery collapse. Global Change Biology 29:2092–2107. https://doi.org/10.1111/gcb.16575

Trainer VL, Moore SK, Hallegraeff G, et al (2020) Pelagic harmful algal blooms and climate change: Lessons from nature's experiments with extremes. Harmful Algae 91:101591. https://doi.org/10.1016/j.hal.2019.03.009

USEPA (2004) Ambient Water Quality Criteria for Dissolved Oxygen, Water Clarity and Chlorophyll a for the Chesapeake Bay and Its Tidal Tributaries

Valle-Levinson A (1995) Observations of barotropic and baroclinic exchanges in the lower Chesapeake Bay. Continental Shelf Research 15:1631–1647. https://doi.org/10.1016/0278-4343(95)00011-O

Valle-Levinson A, Wong K-C, Bosley KT (2001) Observations of the wind-induced exchange at the entrance to Chesapeake Bay. Journal of Marine Research 59:391–416. https://doi.org/10.1357/002224001762842253

Wang D-P (1979) Wind-Driven Circulation in the Chesapeake Bay, Winter 1975. Journal of Physical Oceanography9 9:564–572

Xiong J, Shen J (2022) Vertical Transport Timescale of Surface-Produced Particulate Material in the Chesapeake Bay. JGR Oceans 127:. https://doi.org/10.1029/2021JC017592

Xiong J, Shen J, Qin Q (2021) Exchange Flow and Material Transport Along the Salinity Gradient of a Long Estuary. JGR Oceans 126:. https://doi.org/10.1029/2021JC017185

Xiong Y, Berger CR (2010) Chesapeake Bay Tidal Characteristics. JWARP 2:10

Zhong L, Li M (2006) Tidal energy fluxes and dissipation in the Chesapeake Bay. Continental Shelf Research 26:752–770. https://doi.org/10.1016/j.csr.2006.02.006